

Scaling theory of continuum dislocation dynamics in three dimensions: Self-organized fractal pattern formation

Yong S. Chen, Woosong Choi, Stefanos Papanikolaou, Matthew Bierbaum and James P. Sethna
*Laboratory of Atomic and Solid State Physics (LASSP),
Clark Hall, Cornell University, Ithaca, New York 14853-2501, USA*

We study the morphology of plastic deformation by using a continuum dislocation dynamics theory (CDD) in three dimensions (3D). We study three distinct physically motivated dynamics which consistently lead to fractal formation in 3D with rather similar morphologies, and therefore we suggest that this is a general feature of the 3D collective behavior of dislocations. The striking self-similar features are measured in terms of correlation functions of physical observables, such as the geometrically necessary dislocation (GND) density, the plastic distortion, and the crystalline orientation. Remarkably, all these correlation functions exhibit spatial power-law behaviors, sharing a single underlying universal critical exponent for each type of dynamics.

PACS numbers: 61.72.Bb, 61.72.Lk, 05.45.Df, 05.45.Pq

I. INTRODUCTION

Dislocations in plastically deformed crystals, driven by their long-range interactions, collectively evolve into complex heterogeneous structures where dislocation-rich cell walls or boundaries surround dislocation-depleted cell interiors. These have been observed both in single crystals^{1–3} and polycrystals⁴ using transmission electron microscopy (TEM). The mesoscopic cellular structures have been recognized as scale-free patterns through fractal analysis of TEM micrographs^{5–8}. The complex collective behavior of dislocations has been a challenge for understanding the underlying physical mechanisms responsible for the development of emergent dislocation morphologies.

Complex dislocation microstructures, as an emergent mesoscale phenomenon, have been previously modeled using various theoretical and numerical approaches. Discrete dislocation dynamics (DDD) models have provided insights into the dislocation pattern formations: parallel edge dislocations in a two-dimensional system evolve into ‘matrix structures’ during single slip⁹, and ‘fractal and cell structures’ during multiple slip^{10,11}; random dislocations in a three-dimensional system self-organize themselves into microstructures through junction formation, cross-slip, and short-range interactions^{12,13}. However, DDD simulations are limited by the computational challenges on the relevant scales of length and strain. Beyond these micro-scale descriptions, CDD has also been used to study complex dislocation structures. Simplified reaction-diffusion models have described persistent slip bands¹⁴, dislocation cellular structures during multiple slip¹⁵, and dislocation vein structures¹⁶. Stochasticity in CDD models^{7,9,17} or in the splittings and rotations of the macroscopic cells^{18–20} have been suggested as an explanation for the formation of organized dislocation structures. The source of the noise in these stochastic theories is derived from either extrinsic disorder or short-length-scale fluctuations.

In a recent manuscript²¹, we analyzed the behavior

of a grossly simplified continuum dislocation model for plasticity^{21–24} – a physicist’s ‘spherical cow’ approximation designed to explore the minimal ingredients necessary to explain key features of the dynamics of deformation. Our simplified model ignores many features known to be important for cell boundary morphology and evolution, including slip systems and crystalline anisotropy, dislocation nucleation, lock formation and entanglement, line tension, geometrically unnecessary forest dislocations, etc. However, our model does encompass a realistic order parameter field (the Nye dislocation density tensor²⁵ embodying the GNDs), which allows detailed comparisons of local rotations and deformations, stress, and strain. It is not a realistic model of a real material, but it is a model material with a physically sensible evolution law. Given these simplifications, our model exhibited a surprisingly realistic evolution of cellular structures. We analyzed these structures in two-dimensional simulations (full three-dimensional rotations and deformations, but uniform along the z -axis) using both the fractal box counting method^{5–8} and the single-length-scale scaling methods^{26–29} used in previous theoretical analyses of experimental data. Our model qualitatively reproduced the self-similar, fractal patterns found in the former, and the scaling behavior of the cell sizes and misorientations under strain found in the latter (power-law refinement of the cell sizes, power-law increases in misorientations, and scaling collapses of the distributions).

There are many features of real materials which are not explained by our model. We do not observe distinctions between ‘geometrically necessary’ and ‘incidental’ boundaries, which appear experimentally to scale in different ways. The fractal scaling observed in our model may well be cut off or modified by entanglement, slip-system physics, quantization of Burger’s vector³⁰ or anisotropy – we cannot predict that real materials should have fractal cellular structures; we only observe that our model material does so naturally. Our spherically symmetric model obviously cannot reproduce the dependence of morphological evolution on the axis of applied

strain (and hence the number of activated slip systems); indeed, the fractal patterns observed in some experiments^{7,8} could be associated with the high-symmetry geometry they studied^{31,32}. While many realistic features of materials that we ignore may be important for cell-structure formation and evolution, our model gives clear evidence that these features are not essential to the formation of cellular structures when crystals undergo plastic deformation.

In this longer manuscript, we provide an in-depth analysis of three plasticity models. We show how they (and more traditional models) can be derived from the structures of the broken symmetries and order parameters. We extend our simulations to 3D, where the behavior is qualitatively similar with a few important changes. Here we focus our attention on relaxation (rather than strain), and on correlation functions (rather than fractal box counting or cell sizes and misorientations).

Our model exhibits fractal cell structures directly upon relaxation from randomly deformed initial conditions (Sec. III B). This is not the case for realistic materials, where the dislocation evolution cannot be postponed to start after the plastic deformation is imposed. Indeed, cellular structures in real materials emerge only after significant deformation; presumably this feature is missing in our model because our model has no impediment to cross-slip or multiple slip, and no entanglement of dislocations. This initial relaxation should not be viewed as annealing or dislocation creep. A proper description of annealing must include dislocation line tension effects, since the driving force for annealing is the reduction in total dislocation density – our dislocations annihilate when their Nye Burger’s vector density cancels under evolution, not because of the dislocation core energies. Creep involves dislocation climb, which (for two of our three models) is forbidden. Instead, we view this initial relaxation as the evolution under an instantaneous external plastic deformation – the dislocations produced by random, rapid hammer blows (Sec. III B). The resulting cellular structures are qualitatively very similar to those we observe under external strain^{21,33}, except that they are statistically isotropic. Indeed, we believe that the relaxation evolution we study here mimics almost precisely what we would observe under an imposed time-increasing random plastic deformation from an initially uniform state – slow hammer blows producing similar patterns to relaxation after rapid ones.

We focus here on correlation functions, rather than the methods used in previous analyses of experiments. Correlation functions have a long, dignified history in the study of systems exhibiting emergent scale invariance – materials at continuous thermodynamic phase transitions³⁴, fully developed turbulence^{35,36}, and crackling noise and self-organized criticality³⁷. We study not only numerical simulations of these correlations, but provide also extensive analysis of the relations between the correlation functions for different physical quantities and their (possibly universal) power-law exponents. The decom-

position of the system into cells (needed for the cell-size and misorientation distribution analyses^{26–29}) demands the introduction of an artificial cutoff misorientation angle, and demands either laborious human work or rather sophisticated numerical algorithms³⁸. These sections of the current manuscript may be viewed both as a full characterization of the behavior of our simple model, and as an illustration of how one can use correlation functions to analyze the complex morphologies in more realistic models and in experiments providing 2D or 3D real-space data. We believe that analyses that explicitly decompose structures into cells remain important for systems with single changing length-scale: grain boundary coarsening should be studied both with correlation functions and with explicit studies of grain shape and geometry evolution, and the same should apply to cell-structure models and experiments that are not fractal. But our model, without such an intermediate length-scale, is best analyzed using correlation functions.

Our earlier work²¹ focused on 2D. How different are our predictions in 3D? In this paper, we explore three different CDDs that display similar dislocation fractal formation in 3D and confirm analytically that correlation functions of the GND density, the plastic distortion, and the crystalline orientation, all share a single underlying critical exponent, up to exponent relations, dependent only on the type of dynamics. Unlike our 2D simulations, where forbidding climb led to rather distinct critical exponents, all three dynamics in 3D share quite similar scaling behaviors.

We begin our discussion in Sec. II A by defining the various dislocation, distortion, and orientation fields. In Sec. II B, we derive standard local dynamical evolution laws using traditional condensed matter approaches, starting from both the non-conserved plastic distortion and the conserved GND densities as order parameters. Here, we also explain why these resulting dynamical laws are inappropriate at the mesoscale. In Sec. II C, we show how to extend this approach by defining appropriate constitutive laws for the dislocation flow velocity to build novel dynamics³⁹. There are three different dynamics we study: i) isotropic climb-and-glide dynamics (CGD)^{22–24,40,41}, ii) isotropic glide-only dynamics, where we define the part of the local dislocation density that participates in the local *mobile dislocation population*, keeping the local volume conserved at all times (GOD-MDP)²¹, iii) isotropic glide-only dynamics, where glide is enforced by a *local vacancy pressure* due to a co-existing background of vacancies that have an infinite energy cost (GOD-LVP)⁴². All three types of dynamics present physically valid alternative approaches for deriving a coarse-grained continuum model for GNDs. In Sec. III, we discuss the details of numerical simulations in both two and three dimensions, and characterize the self-organized critical complex patterns in terms of correlation functions of the order parameter fields. In Sec. IV, we provide a scaling theory, and derive relations among the critical exponents of these related correlation func-

tions, and conclude in Sec. V.

In addition, we provide extensive details of our study in Appendices. In Appendix A, we collect useful formulas from the literature relating different physical quantities within traditional plasticity, while in Appendix B we show how functional derivatives and the dissipation rate can be calculated using this formalism, leading to our proof that our CDDs are strictly dissipative (lowering the appropriate free energy with time). In Appendix C, we show the flexibility of our CDDs by extending our dynamics: In particular, we show how to add vacancy diffusion in the structure of CDD, and also, how external disorder can be in principle incorporated (to be explored in future work). In Appendix D, we elaborate on numerical details – we demonstrate the statistical convergence of our simulation method and also we explain how we construct the Gaussian random initial conditions. Finally, in Appendix E, we discuss the scaling properties of several correlation functions in real and Fourier spaces, including the strain-history-dependent plastic deformation and distortion fields, the stress-stress correlation functions, the elastic energy density spectrum, and the stressful part of GND density.

II. CONTINUUM MODELS

A. Order parameter fields

1. Conserved order parameter field

A dislocation is the topological defect of a crystal lattice. In a continuum theory, it can be described by a coarse-grained variable, the GND density⁴³, (also called the net dislocation density or the Nye dislocation density), which can be defined by the GND density tensor

$$\rho(\mathbf{x}) = \sum_{\alpha} (\hat{\mathbf{t}}^{\alpha} \cdot \hat{\mathbf{n}}) \hat{\mathbf{n}} \otimes \mathbf{b}^{\alpha} \delta(\mathbf{x} - \boldsymbol{\xi}^{\alpha}), \quad (1)$$

so

$$\rho_{km}(\mathbf{x}) = \sum_{\alpha} \hat{t}_k^{\alpha} b_m^{\alpha} \delta(\mathbf{x} - \boldsymbol{\xi}^{\alpha}), \quad (2)$$

measuring the sum of the net flux of dislocations α located at $\boldsymbol{\xi}$, tangent to $\hat{\mathbf{t}}$, with Burgers vector \mathbf{b} , in the neighborhood of \mathbf{x} , through an infinitesimal plane with the normal direction along $\hat{\mathbf{n}}$, seen in Fig. 1. In the continuum, the discrete sum of line singularities in Eqs. (1) and (2) is smeared into a continuous (nine-component) field, just as the continuum density of a liquid is at root a sum of point contributions from atomic nuclei.

Since the normal unit pseudo-vector $\hat{\mathbf{n}}$ is equivalent to an antisymmetric unit bivector \hat{E} , $\hat{E}_{ij} = \varepsilon_{ijk} \hat{n}_k$, we can reformulate the GND density as a three-index tensor

$$\varrho(\mathbf{x}) = \sum_{\alpha} (\hat{\mathbf{t}}^{\alpha} \cdot \hat{\mathbf{n}}) \hat{E} \otimes \mathbf{b}^{\alpha} \delta(\mathbf{x} - \boldsymbol{\xi}^{\alpha}), \quad (3)$$

so

$$\varrho_{ijm}(\mathbf{x}) = \sum_{\alpha} (\hat{t}_i^{\alpha} \hat{n}_l) \hat{E}_{ij} b_m^{\alpha} \delta(\mathbf{x} - \boldsymbol{\xi}^{\alpha}), \quad (4)$$

measuring the same sum of the net flux of dislocations in the neighborhood of \mathbf{x} , through the infinitesimal plane indicated by the unit bivector \hat{E} . This three-index variant will be useful in Sec. II C 2, where we adapt the equations of Refs. 23 and 24 to forbid dislocation climb (GOD-MDP).

According to the definition of \hat{E} , we can find the relation between ρ and ϱ

$$\varrho_{ijm}(\mathbf{x}) = \sum_{\alpha} (\hat{t}_i^{\alpha} \hat{n}_l) \varepsilon_{ijk} \hat{n}_k b_m^{\alpha} \delta(\mathbf{x} - \boldsymbol{\xi}^{\alpha}) = \varepsilon_{ijk} \rho_{km}(\mathbf{x}). \quad (5)$$

It should be noted here that dislocations cannot terminate within the crystal, implying that

$$\partial_i \rho_{ij}(\mathbf{x}) = 0, \quad (6)$$

or

$$\varepsilon_{ijk} \partial_k \varrho_{ijl}(\mathbf{x}) = 0. \quad (7)$$

Within plastic theories, the gradient of the total displacement field \mathbf{u} represents the compatible total distortion field⁴⁴ $\beta_{ij} = \partial_i u_j$, which is the sum of the elastic and the plastic distortion fields⁴⁴, $\beta = \beta^p + \beta^e$. Due to the presence of dislocation lines, both β^p and β^e are incompatible, characterized by the GND density ρ

$$\rho_{ij} = \varepsilon_{ilm} \partial_l \beta_{mj}^e, \quad (8)$$

$$= -\varepsilon_{ilm} \partial_l \beta_{mj}^p. \quad (9)$$

The elastic distortion field β^e is the sum of its symmetric strain and antisymmetric rotation fields,

$$\beta^e = \epsilon^e + \omega^e, \quad (10)$$

where we assume linear elasticity, ignoring the ‘geometric nonlinearity’ in these tensors. Substituting the sum of two tensor fields into the incompatibility relation Eq. (8) gives

$$\rho_{ij} = \varepsilon_{ikl} \partial_k \omega_{lj}^e + \varepsilon_{ikl} \partial_k \epsilon_{lj}^e. \quad (11)$$

The elastic rotation tensor ω^e can be rewritten as an axial vector, the crystalline orientation vector $\boldsymbol{\Lambda}$

$$\Lambda_k = \frac{1}{2} \varepsilon_{ijk} \omega_{ij}^e, \quad (12)$$

or

$$\omega_{ij}^e = \varepsilon_{ijk} \Lambda_k. \quad (13)$$

Thus we can substitute Eq. (13) into Eq. (11)

$$\rho_{ij} = (\delta_{ij} \partial_k \Lambda_k - \partial_j \Lambda_i) + \varepsilon_{ikl} \partial_k \epsilon_{lj}^e. \quad (14)$$

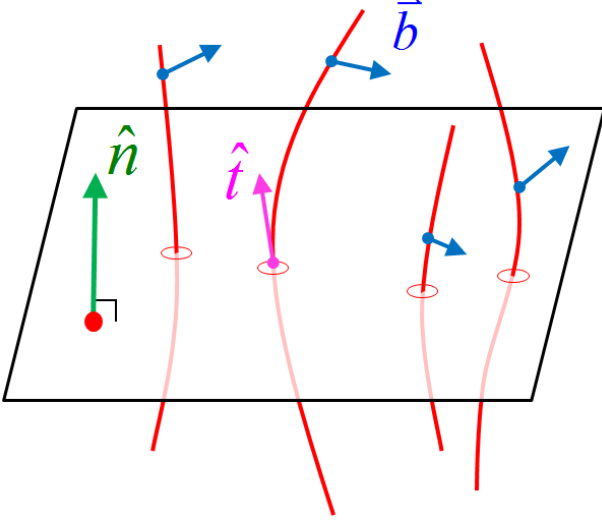


FIG. 1: (Color online) **Representation of the crystalline line defect — dislocation.** Each curved line represents a dislocation line with the tangent direction $\hat{\mathbf{t}}$, and the Burgers vector \mathbf{b} which characterizes the magnitude and direction of the distortion to the lattice. The two-index GND density ρ_{km} (Eqs. 1 and 2) is the net flux of the Burgers vector density \mathbf{b} along $\hat{\mathbf{e}}^{(m)}$ through an infinitesimal piece of a plane with normal direction $\hat{\mathbf{n}}$ along $\hat{\mathbf{e}}^{(k)}$. The three-index version ϱ_{ijm} (Eqs. 3 and 4) is the flux density through the plane along the axes $\hat{\mathbf{e}}^{(i)}$ and $\hat{\mathbf{e}}^{(j)}$, with the unit bivector $\hat{E} = \hat{\mathbf{e}}^{(i)} \wedge \hat{\mathbf{e}}^{(j)}$.

For a system without residual elastic stress, the GND density thus depends only on the varying crystalline orientation⁴⁵.

Dynamically, the time evolution law of the GND density emerges from the conservation of the Burgers vector

$$\frac{\partial}{\partial t} \rho_{ik} = -\varepsilon_{ijq} \partial_j J_{qk}, \quad (15)$$

or

$$\frac{\partial}{\partial t} \varrho_{ijk} = -\varepsilon_{ijm} \varepsilon_{mpq} \partial_p J_{qk} = -g_{ijpq} \partial_p J_{qk}, \quad (16)$$

where J represents the Burgers vector flux, and the symbol g_{ijpq} indicates $\varepsilon_{ijm} \varepsilon_{mpq} = \delta_{ip} \delta_{jq} - \delta_{iq} \delta_{jp}$.

2. Non-conserved order parameter field

The natural physicist's order parameter field ϱ , characterizing the incompatibility, can be written in terms of

the plastic distortion field β^P

$$\varrho_{ijk} = \varepsilon_{ijm} \rho_{mk} = -g_{ijls} \partial_l \beta_{sk}^P. \quad (17)$$

In the linear approximation, the alternative order parameter field β^P fully specifies the local deformation \mathbf{u} of the material, the elastic distortion β^e , the internal long-range stress field σ^{int} and the crystalline orientation (the Rodrigues vector $\mathbf{\Lambda}$ giving the axis and angle of rotation), as summarized in Appendix A.

According to Eq. (9) and Eq. (15), the flux J of the Burgers vector can be expressed in terms of the dynamics of the plastic distortion tensor β^P

$$\frac{\partial \beta_{ij}^P}{\partial t} = J_{ij}. \quad (18)$$

The plastic distortion β^P can be specified by the GND density ρ and a strain-history deformation field ψ in Fourier space⁴⁶,

$$\begin{aligned} \tilde{\beta}_{ij}^P(\mathbf{k}) &= -i\varepsilon_{ilm} \frac{k_l}{k^2} \tilde{\rho}_{mj}(\mathbf{k}) + ik_i \tilde{\psi}_j(\mathbf{k}) \\ &\equiv \tilde{\beta}_{ij}^{P,I}(\mathbf{k}) + \tilde{\beta}_{ij}^{P,H}(\mathbf{k}), \end{aligned} \quad (19)$$

hence decomposing $\tilde{\beta}^P$ into two parts. $\beta^{P,I}$ is the intrinsic field specified by the GND density. Similar to ρ , $\beta^{P,I}$ is also divergence free: $\partial_i \beta_{ij}^{P,I} = 0$, i.e., $k_i \tilde{\beta}_{ij}^{P,I} = 0$. $\beta^{P,H}$ is a (curl-free) gradient of ψ , depending upon the strain history and contributing nothing to the GND density. This decomposition will become important to us in Sec. III C 3, where the correlation functions of $\beta^{P,I}$ and $\beta^{P,H}$ will scale differently with distance.

In the presence of external loading, we can express the appropriate free energy \mathcal{F} as the sum of two terms: the elastic interaction energy of GNDs, and the energy of interaction with the applied stress field. The free energy functional is

$$\mathcal{F} = \int d^3\mathbf{x} \left(\frac{1}{2} \sigma_{ij}^{\text{int}} \epsilon_{ij}^e - \sigma_{ij}^{\text{ext}} \epsilon_{ij}^p \right). \quad (20)$$

Alternatively, it can be rewritten in Fourier space

$$\begin{aligned} \mathcal{F} &= - \int \frac{d^3\mathbf{k}}{(2\pi)^3} \left(\frac{1}{2} M_{ijmn}(\mathbf{k}) \tilde{\beta}_{ij}^P(\mathbf{k}) \tilde{\beta}_{mn}^P(-\mathbf{k}) \right. \\ &\quad \left. + \tilde{\sigma}_{ij}^{\text{ext}}(\mathbf{k}) \tilde{\beta}_{ij}^P(-\mathbf{k}) \right), \end{aligned} \quad (21)$$

as discussed in Appendix B 1.

B. Traditional dissipative continuum dynamics

There are well known approaches for deriving continuum equations of motion for dissipative systems, which in this case produce a traditional von Mises-style theory⁴⁷, useful at longer scales. We begin by reproducing these standard equations.

For the sake of simplicity, we ignore external stress (σ_{ij} simplified to σ_{ij}^{int}) in the following three subsections. We start by using the standard methods applied to the non-conserved order parameter β^p , and then turn to the conserved order parameter ϱ .

1. Dissipative dynamics built from the non-conserved order parameter field β^p

The plastic distortion β^p is a non-conserved order parameter field, which is utilized by the engineering community to study texture evolution and plasticity of mechanically deformed structural materials. The simplest dissipative dynamics in terms of β^p minimizes the free energy by steepest descents

$$\frac{\partial}{\partial t} \beta_{ij}^p = -\Gamma \frac{\delta \mathcal{F}}{\delta \beta_{ij}^p}, \quad (22)$$

where Γ is a positive material-dependent constant. We may rewrite it in Fourier space, giving

$$\frac{\partial}{\partial t} \tilde{\beta}_{ij}^p(\mathbf{k}) = -\Gamma \frac{\delta \mathcal{F}}{\delta \tilde{\beta}_{ij}^p(-\mathbf{k})}. \quad (23)$$

The functional derivative $\delta \mathcal{F} / \delta \tilde{\beta}_{ij}^p(-\mathbf{k})$ is the negative of the long-range stress

$$\frac{\delta \mathcal{F}}{\delta \tilde{\beta}_{ij}^p(-\mathbf{k})} = -M_{ijmn}(\mathbf{k}) \tilde{\beta}_{mn}^p(\mathbf{k}) \equiv -\tilde{\sigma}_{ij}(\mathbf{k}). \quad (24)$$

This dynamics implies a simplified version of von Mises plasticity

$$\frac{\partial}{\partial t} \tilde{\beta}_{ij}^p(\mathbf{k}) = \Gamma \tilde{\sigma}_{ij}(\mathbf{k}). \quad (25)$$

2. Dissipative dynamics built from the conserved order parameter field ϱ

We can also derive an equation of motion starting from the GND density ϱ , as was done by Rickman and Viñals⁴⁷. For this dissipative dynamics Eq. (16), the simplest expression for J is

$$J_{qk} = -\Gamma'_{ablq} \partial_l \frac{\delta \mathcal{F}}{\delta \varrho_{abk}}, \quad (26)$$

where the material-dependent constant tensor Γ' must be chosen to guarantee a decrease of the free energy with time.

The infinitesimal change of \mathcal{F} with respect to the GND density ϱ is

$$\delta \mathcal{F}[\varrho] = \int d^3 \mathbf{x} \frac{\delta \mathcal{F}}{\delta \varrho_{ijk}} \delta \varrho_{ijk}. \quad (27)$$

The free energy dissipation rate is thus $\delta \mathcal{F} / \delta t$ for $\delta \varrho = \frac{\partial \varrho}{\partial t} \delta t$, hence

$$\frac{\partial}{\partial t} \mathcal{F}[\varrho] = \int d^3 \mathbf{x} \frac{\delta \mathcal{F}}{\delta \varrho_{ijk}} \frac{\partial \varrho_{ijk}}{\partial t}. \quad (28)$$

Substituting Eq. (16) into Eq. (28) and integrating by parts gives

$$\frac{\partial}{\partial t} \mathcal{F}[\varrho] = \int d^3 \mathbf{x} \left(g_{ijpq} \partial_p \frac{\delta \mathcal{F}}{\delta \varrho_{ijk}} \right) J_{qk}. \quad (29)$$

Substituting Eq. (26) into Eq. (29) gives

$$\frac{\partial}{\partial t} \mathcal{F}[\varrho] = - \int d^3 \mathbf{x} \left(g_{ijpq} \partial_p \frac{\delta \mathcal{F}}{\delta \varrho_{ijk}} \right) \left(\Gamma'_{ablq} \partial_l \frac{\delta \mathcal{F}}{\delta \varrho_{abk}} \right). \quad (30)$$

Now, to guarantee that energy never increases, we choose $\Gamma'_{ablq} = \Gamma g_{ablq}$, (Γ is a positive material-dependent constant), which yields the rate of change of energy as a negative of a perfect square

$$\frac{\partial}{\partial t} \mathcal{F}[\varrho] = - \int d^3 \mathbf{x} \Gamma \sum_{q,k} \left(g_{ablq} \partial_l \frac{\delta \mathcal{F}}{\delta \varrho_{abk}} \right)^2. \quad (31)$$

Using Eqs. (16) and (26), we can write the dynamics in terms of ϱ

$$\frac{\partial}{\partial t} \varrho_{ijk} = \Gamma g_{ijpq} g_{ablq} \partial_p \partial_l \frac{\delta \mathcal{F}}{\delta \varrho_{abk}}. \quad (32)$$

Substituting the functional derivative $\delta \mathcal{F} / \delta \varrho_{abk}$, Eq. (B10), derived in Appendix B 2, into Eq. (32) and comparing to Eq. (16) tells us

$$\frac{\partial}{\partial t} \varrho_{ijk}(\mathbf{x}) = -\Gamma g_{ijpq} \partial_p \sigma_{qk}(\mathbf{x}) = -g_{ijpq} \partial_p J_{qk}(\mathbf{x}), \quad (33)$$

where

$$J_{qk} = \Gamma \sigma_{qk} \quad (34)$$

duplicating the von Mises law (Eq. 25) of the previous subsection. The simplest dissipative dynamics of either non-conserved or conserved order parameter fields thus turns out to be the traditional linear dynamics, a simplified von Mises law.

The problem with this law for us is that it allows for plastic deformation in the absence of dislocations, i.e., the Burgers vector flux can be induced through the elastic loading on the boundaries, even in a defect-free medium. This is appropriate on engineering length scales above or around a micron, where statistically stored dislocation (SSD) dominates the plastic deformation. (Methods to incorporate their effects into a theory like ours have been provided by Acharya *et al.*^{42,48} and Varadhan *et al.*⁴⁹)

By ignoring the SSDs, our theory assumes that there is an intermediate coarse-graining length scale, large compared to the distance between dislocations and small

compared to the distance where the cancelling of dislocations with different Burger’s vectors dominates the dynamics. We believe this latter length scale is given by the distance between cell walls (as discussed in Sec. III B). The cell wall misorientations are geometrically necessary. On the one hand, it is known^{50,51} that neighboring cell walls often have misorientations of alternating signs, so that on coarse-grained length scales just above the cell wall separation one would expect explicit treatment of the SSDs would be necessary. On the other hand, the density of dislocations in cell walls is high, so that a coarse-graining length much smaller than the interesting structures (and hence where we believe SSDs are unimportant) should be possible. (Our cell structures are fractal, with no characteristic ‘cell size’; this coarse-graining length sets the minimum cutoff scale of the fractal, and the grain size or inhomogeneity length will set the maximum scale.) With this assumption, to treat the formation of cellular structures, we turn to theories of the form given in Eq. (15), defined in terms of dislocation currents J that depend directly on the local GND density.

C. Our CDD model

The microscopic motion of a dislocation under external strain depends upon temperature. In general, it moves quickly along the glide direction, and slowly (or not at all) along the climb direction where vacancy diffusion must carry away the atoms. The glide speed can be limited by phonon drag at higher temperatures, or can accelerate to nearly the speed of sound at low temperatures⁵². It is traditional to assume that the dislocation velocity is over-damped, and proportional to the component of the force per unit dislocation length in the glide plane.

To coarse-grain this microscopics, for reasons described above, we choose a CDD model whose dislocation currents vanish when the GND density vanishes. Limkumnerd and Sethna²⁴ derived a dislocation current J for this case using a closure approximation of the underlying microscopics. Their work reproduced (in the case of both glide and climb) an earlier dynamical model proposed by Acharya and collaborators^{22,23} assuming a single velocity field for the dislocations.

In our CGD and GOD-LVP dynamics (Sections II C 1 and II C 3 below), we also assume that all dislocations in the infinitesimal volume at \mathbf{x} are moving with a common velocity $\mathbf{v}(\mathbf{x})$. This common velocity ansatz was first mentioned by Mura⁵³, but as a warning that it is an incorrect assumption. Microscopically, different dislocations in a region experience Peach-Koehler forces in different directions, and will not move in tandem. (In real materials the dislocation dynamics is intermittent, as dislocations bow out or depin from junctions and disorder, and engage in complex dislocation avalanches. Our model has no pinning and hence no metastability: the single velocity approximation is an additional assumption.) Indeed, it is the difference in velocities for dislo-

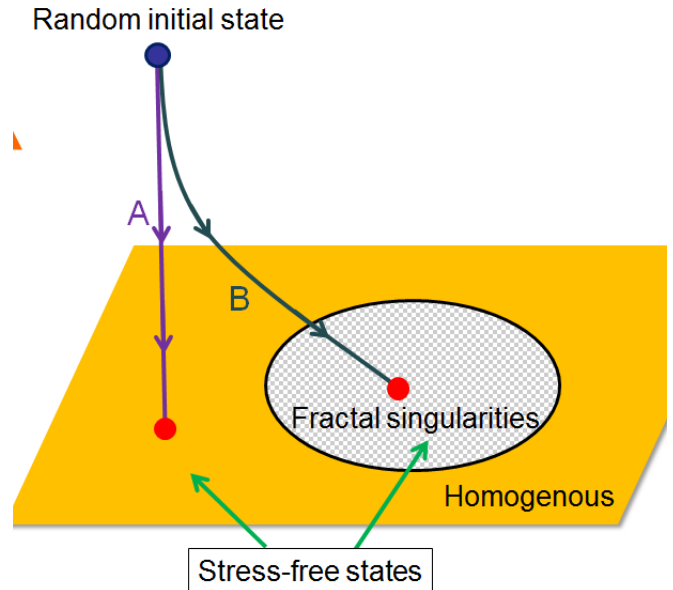


FIG. 2: (Color online) **Relaxation of various CDD models.** The blue dot represents the initial random plastically-deformed state; the red dots indicate the equilibrated stress-free states driven by different dynamics. Curve A: steepest decent dynamics leads to the trivial homogeneous equilibrated state, discussed in Sec. II B. Curve B: our CDD models settle the system into non-trivial stress-free states with wall-like singularities of the GND density, discussed in Sec. II C.

cations on different slip systems that leads to entanglement. It is also not justified in a coarse-grained theory (unlike fluid mechanics, where momentum conservation and Galilean invariance leads to an emergent collective local velocity for systems in local equilibrium). However, we shall see that variants of the local velocity ansatz allow one to construct physically sensible ‘model materials’ – perhaps not the correct theory for a particular material, but a sensible framework to generate theories of plastic deformation. This ansatz has been supplemented by constitutive laws for the velocity field by Acharya²² and collaborators^{23,40–42,49} to generate CDD theories. We follow their argument in Sec. II C 1 to derive the dynamics allowing both glide and climb, and then modify it to remove climb in Sec. II C 2. We also derive a second variant version of glide-only dynamics in Sec. II C 3 by approaching the limit of infinite vacancy energy, which reproduces a model proposed by Acharya and Roy⁴².

1. Climb-glide dynamics (CGD)

We start with a model presuming (perhaps unphysically) that vacancy diffusion is so fast that dislocations climb and glide with equal mobility. The elastic Peach-Koehler force due to the stress $\sigma(\mathbf{x})$ on the local GND density is given by $\mathbf{f}_u^{PK} = \sigma_{mk}\varrho_{umk}$. We assume that the velocity $\mathbf{v} \propto \mathbf{f}^{PK}$, giving a local constitutive relation

$$v_u \propto \sigma_{mk}\varrho_{umk}. \quad (35)$$

How should we determine the proportionality constant between velocity and force? In experimental systems, this is complicated by dislocation entanglement and short-range forces between dislocations. Ignoring these features, the velocity of each dislocation should depend only on the stress induced by the other dislocations, not the local density of dislocations⁵⁴. We can incorporate this in an approximate way by making the proportionality factor in Eq. (35) inversely proportional to the GND density. We measure the latter by summing the square of all components of ϱ , hence $|\varrho| = \sqrt{\varrho_{ijk}\varrho_{ijk}/2}$ and $v_u = \frac{D}{|\varrho|}\sigma_{mk}\varrho_{umk}$, where D is a positive material-dependent constant. This choice has the additional important feature that the evolution of a sharp domain wall whose width is limited by the lattice cutoff is unchanged when the lattice cutoff is reduced.

The flux J of the Burgers vector is thus

$$J_{ij} = v_u\varrho_{uij} = \frac{D}{|\varrho|}\sigma_{mk}\varrho_{umk}\varrho_{uij}. \quad (36)$$

Notice that this dynamics satisfies our criterion that $J = 0$ when there are no GNDs (i.e., $\varrho = 0$).

Substituting this flux J (Eq. 36) into the free energy dissipation rate (Eq. B16) gives

$$\frac{\partial\mathcal{F}}{\partial t} = - \int d^3\mathbf{x} \sigma_{ij}J_{ij} = - \int d^3\mathbf{x} \frac{|\varrho|}{D}v^2 \leq 0. \quad (37)$$

Details are given in Appendix B3.

2. Glide-only dynamics: mobile dislocation population (GOD-MDP)

When the temperature is low enough, dislocation climb is negligible, i.e., dislocations can only move in their glide planes. Fundamentally, dislocation glide conserves the total number of atoms, which leads to an unchanged local volume. Since the local volume change in time is represented by the trace J_{ii} of the flux of the Burgers vector, conservative motion of GNDs demands $J_{ii} = 0$. Limkumnerd and Sethna²⁴ derived the equation of motion for dislocation glide only, by removing the trace of J from Eq. (36). However, their dynamics fails to guarantee that the free energy monotonically decreases. Here we present an alternative approach.

We can remove the trace of J by modifying the first equality in Eq. (36),

$$J'_{ij} = v'_u \left(\varrho_{uij} - \frac{1}{3}\delta_{ij}\varrho_{ukk} \right), \quad (38)$$

where $\varrho'_{uij} = \varrho_{uij} - \frac{1}{3}\delta_{ij}\varrho_{ukk}$ can be viewed as a subset of ‘mobile’ dislocations moving with velocity \mathbf{v}' .

Substituting the current (Eq. 38) into the free energy dissipation rate (Eq. B16) gives

$$\frac{\partial\mathcal{F}}{\partial t} = - \int d^3\mathbf{x} \sigma_{ij}(v'_u\varrho'_{uij}). \quad (39)$$

If we choose the velocity $v'_u \propto \sigma_{ij}\varrho'_{uij}$, the appropriate free energy monotonically decreases in time. We thus express $v'_u = \frac{D}{|\varrho|}\varrho'_{uij}\sigma_{ij}$, where D is a positive material-dependent constant, and the prefactor $1/|\varrho|$ is added for the same reasons, as discussed in the second paragraph of Sec. II C 1.

The current J' of the Burgers vector is thus written²¹

$$\begin{aligned} J'_{ij} &= v'_u\varrho'_{uij} \\ &= \frac{D}{|\varrho|}\sigma_{mn} \left(\varrho_{umn} - \frac{1}{3}\delta_{mn}\varrho_{ull} \right) \left(\varrho_{uij} - \frac{1}{3}\delta_{ij}\varrho_{ukk} \right). \end{aligned} \quad (40)$$

This natural evolution law becomes much less self-evident when expressed in terms of the traditional two-index version ρ (Eqs. 1&2)

$$\begin{aligned} J'_{ij} &= \frac{D}{|\varrho|} \left(\sigma_{in}\rho_{mn}\rho_{mj} - \sigma_{mn}\rho_{in}\rho_{mj} - \frac{1}{3}\sigma_{mm}\rho_{ni}\rho_{nj} \right. \\ &\quad \left. + \frac{1}{3}\sigma_{mm}\rho_{in}\rho_{nj} - \frac{\delta_{ij}}{3} \left(\sigma_{kn}\rho_{mn}\rho_{mk} - \sigma_{mn}\rho_{kn}\rho_{mk} \right. \right. \\ &\quad \left. \left. - \frac{1}{3}\sigma_{mm}\rho_{nk}\rho_{nk} + \frac{1}{3}\sigma_{mm}\rho_{kn}\rho_{nk} \right) \right), \end{aligned} \quad (41)$$

(which is why we introduce the three-index variant ϱ).

This current J' makes the free energy dissipation rate the negative of a perfect square in Eq. (B18). Details are given in Appendix B3.

3. Glide-only dynamics: local vacancy-induced pressure (GOD-LVP)

At high temperature, the fast vacancy diffusion leads to dislocation climb out of the glide direction. As the temperature decreases, vacancies are frozen out so that dislocations only slip in the glide planes. In Appendix C 1, we present a dynamical model coupling the vacancy diffusion to our CDD model. Here we consider the limit of frozen-out vacancies with infinite energy costs, which leads to another version of glide-only dynamics.

According to the coupling dynamics Eq. (C8), we write down the general form of dislocation current

$$J''_{ij} = \frac{D}{|\varrho|} \left(\sigma_{mn} - \delta_{mn} p \right) \varrho_{umn} \varrho_{uij}, \quad (42)$$

where p is the local pressure due to vacancies.

The limit of infinitely costly vacancies ($\alpha \rightarrow \infty$ in Appendix C 1) leads to the traceless current, $J''_{ii} = 0$. Solving this equation gives a critical local pressure p^c

$$p^c = \frac{\sigma_{pq} \varrho_{spq} \varrho_{skk}}{\varrho_{uaa} \varrho_{ubb}}. \quad (43)$$

The corresponding current J'' of the Burgers vector in this limit is thus written

$$J''_{ij} = \frac{D}{|\varrho|} \left(\sigma_{mn} - \frac{\sigma_{pq} \varrho_{spq} \varrho_{skk}}{\varrho_{uaa} \varrho_{ubb}} \delta_{mn} \right) \varrho_{umn} \varrho_{uij}, \quad (44)$$

reproducing the glide-only dynamics proposed by Acharya and Roy⁴².

Substituting the current (Eq. 44) into the free energy dissipation rate (Eq. B16) gives

$$\frac{\partial \mathcal{F}}{\partial t} = - \int d^3 \mathbf{x} \frac{D}{|\varrho|} \left[f_i^{PK} f_i^{PK} - \left(\frac{d_i f_i^{PK}}{|\mathbf{d}|} \right)^2 \right] \leq 0, \quad (45)$$

where $f_i^{PK} = \sigma_{mn} \varrho_{imn}$ and $d_i = \varrho_{ikk}$. The equality emerges when the force \mathbf{f}^{PK} is along the same direction as \mathbf{d} .

Unlike the traditional linear dissipative models, our CDD model, coarse grained from microscopic interactions, drives the random plastic distortion to non-trivial stress-free states with dislocation wall singularities, as schematically illustrated in Fig. 2.

Our minimal CDD model, consisting of GNDs evolving under the long-range interaction, provides a framework for understanding dislocation morphologies at the mesoscale. Eventually, it can be extended to include vacancies by coupling them to the dislocation current (as discussed in Appendix C 1, or extended to include disorder, dislocation pinning, and entanglement by adding appropriate interactions to the free energy functional and refining the effective stress field (as discussed in Appendix C 2). It has already been extended to include SSDs incorporating traditional crystal plasticity theories^{42,48,49}.

III. RESULTS

A. Two and three dimensional simulations

We perform simulations in 2D and 3D the dislocation dynamics of Eq. (15) and Eq. (18), with dynamical currents defined by CGD (Eq. 36), GOD-MDP (Eq. 40), and GOD-LVP (Eq. 44). We numerically observe that

simulations of Eqs. (15), (18) lead to the same results statistically (i.e., the numerical time step approximations leave the physics invariant). We therefore focus our presentation on the results of Eq. (18), where the evolving field variable β^p is unconstrained. Our CGD and GOD-MDP models have been quite extensively simulated in one and two dimensions and relevant results can be found in Refs. 21, 24, and 55. In this paper, we concentrate on periodic grids of spatial extent L in both two²¹ and three dimensions. The numerical approach we use is a second-order central upwind scheme designed for Hamilton-Jacobi equations⁵⁶ using finite differences. This method is quite efficient in capturing δ -shock singular structures³⁶, even though it is flexible enough to allow for the use of approximate solvers near the singularities.

Our numerical simulations show a close analogy to those of turbulent flows³⁶. As in three-dimensional turbulence, defect structures lead to intermittent transfer of morphology to short length scales. As conjectured^{57,58} for the Euler equations or the inviscid limit of Navier-Stokes equations, our simulations develop singularities in finite time^{21,24}. Here these singularities are δ -shocks representing grain-boundary-like structures emerging from the mutual interactions among mobile dislocations⁵⁹. In analogy with turbulence, where the viscosity serves to smooth out the vortex-stretching singularities of the Euler equations, we have explored the effects of adding an artificial viscosity term to our equations of motion³⁶. In the presence of artificial viscosity, our simulations exhibit nice numerical convergence in all dimensions⁵⁹. However, in the limit of vanishing viscosity, the solutions of our dynamics continue to depend on the lattice cutoff in higher dimensions, (our simulations only exhibit numerical convergence in one dimension). Actually, the fact that the physical system is cut off by the atomic scale leads to the conjecture that our equations are in some sense non-renormalizable in the ultraviolet. These issues are discussed in detail in Refs. 36 and 59.

In the vanishing viscosity limit, our simulations exhibit fractal structure down to the smallest scales. When varying the system size continuously, the solutions of our dynamics exhibit a convergent set of correlation functions of the various order parameter fields, which are used to characterize the emergent self-similarity. This statistical convergence is numerically tested in Appendix D 1.

In both two and three dimensional simulations, we relax the deformed system with and without dislocation climb in the absence of external loading. Here, the initial plastic distortion field β^p is still a Gaussian random field with correlation length scale $\sqrt{2}L/5 \sim 0.28L$ and initial amplitude $\beta_0 = 1$. (In our earlier work²¹, we described this length as $L/5$, using a non-standard definition of correlation length scale; see Appendix D 2.) These random initial conditions are explained in Appendix D 2. In 2D, Figure 3 shows that CGD and GOD-LVP simulations (top and bottom) exhibit much sharper, flatter boundaries than GOD-MDP (middle). This dif-

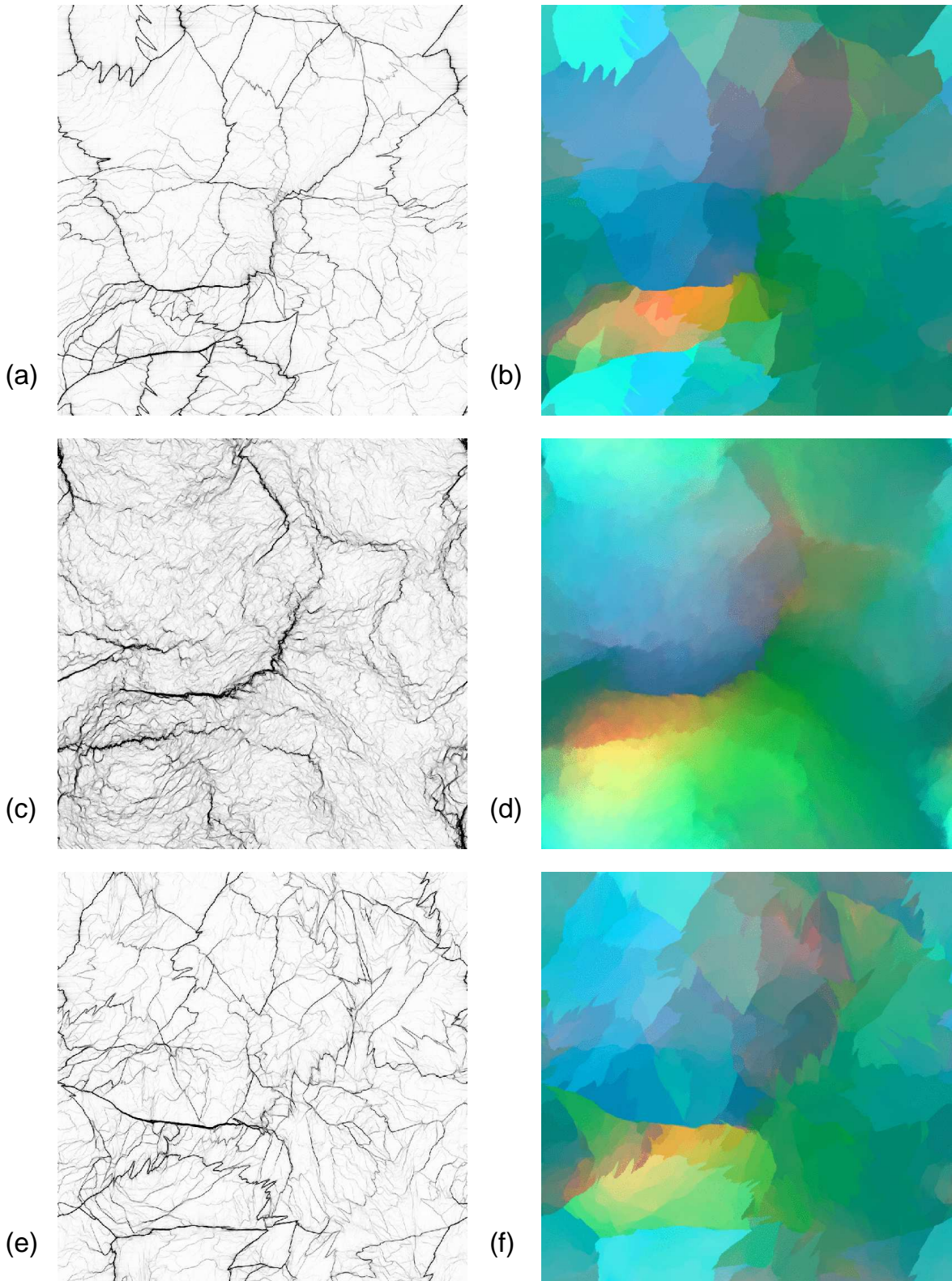


FIG. 3: (Color online) **Complex dislocation structures in two dimensions** (1024^2) for the relaxed states of an initially random distortion. *Top:* Dislocation climb is allowed; *Middle:* Glide only using a mobile dislocation population; *Bottom:* Glide only using a local vacancy pressure. *Left:* Net GND density $|\rho|$ plotted linearly in density with dark regions a factor $\sim 10^4$ more dense than the lightest visible regions. (a) When climb is allowed, the resulting morphologies are sharp, regular, and close to the system scale. (c) When climb is forbidden using a mobile dislocation population, there is a hierarchy of walls on a variety of length scales, getting weaker on finer length scales. (e) When climb is removed using a local vacancy pressure, the resulting morphologies are as sharp as those (a) allowing climb. *Right:* Corresponding local crystalline orientation maps, with the three components of the orientation vector $\mathbf{\Lambda}$ linearly mapped onto a vector of RGB values. Notice the fuzzier cell walls (c) and (d) suggests a larger fractal dimension.

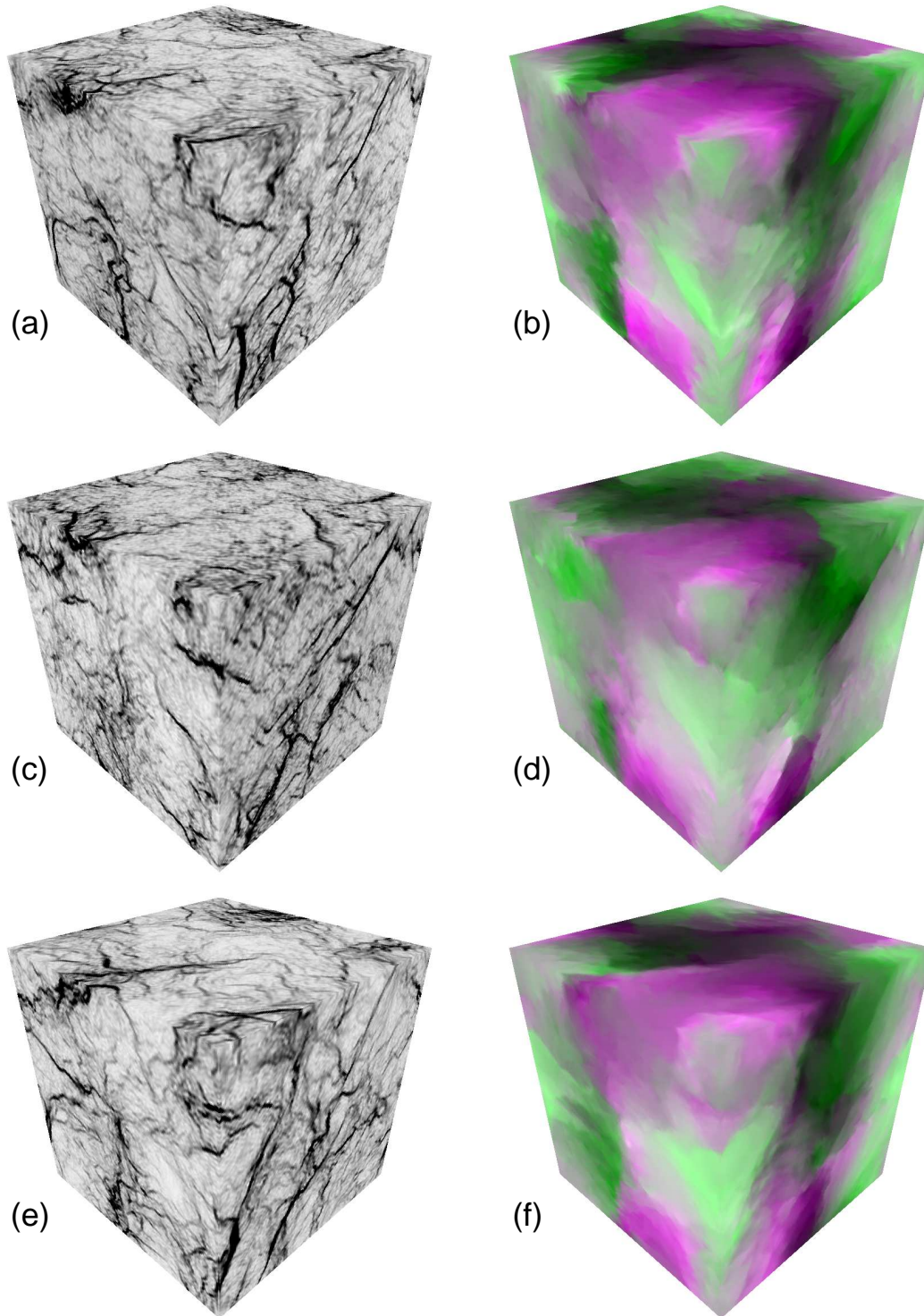


FIG. 4: (Color online) **Complex dislocation structures in three dimensions** (128^3) for the relaxed states of an initially random distortion. Notice these textured views on the surface of simulation cubes. *Top*: Dislocation climb is allowed; *Middle*: Glide only using a mobile dislocation population; *Bottom*: Glide only using a local vacancy pressure. *Left*: Net GND density $|\rho|$ plotted linearly in density with dark regions a factor $\sim 10^3$ more dense than the lightest visible regions. The cellular structures in (a), (c), and (e) seem similarly fuzzy; our theory in three dimensions generates fractal cell walls. *Right*: Corresponding local crystalline maps, with the three components of the orientation vector $\mathbf{\Lambda}$ linearly mapped onto a vector of RGB values.

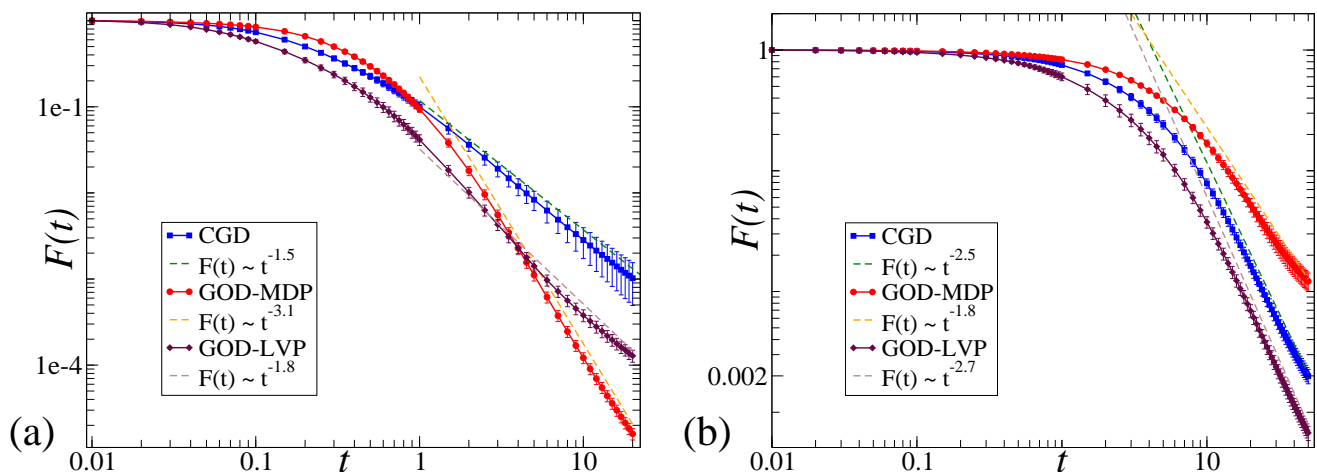


FIG. 5: (Color online) **The elastic free energy decreases to zero as a power law in time in both two and three dimensions.** In both (a) and (b), we show that the free energy \mathcal{F} decays monotonically in time, and goes to zero as a power law for CGD, GOD-MDP, and GOD-LVP simulations, as the system relaxes in the absence of external strain.

ference is quantitatively described by the large shift in the static critical exponent η in 2D for both CGD and GOD-LVP. In our earlier work²¹, we announced this difference as providing a sharp distinction between high-temperature, non-fractal grain boundaries (for CGD), and low-temperature, fractal cell wall structures (for GOD-MDP). This appealing message did not survive the transition to 3D; Figure 4 shows basically indistinguishable complex cellular structures, for all three types of dynamics. Indeed, Table I shows only a small change in critical exponents, among CGD, GOD-MDP, and GOD-LVP. During both two and three dimensional relaxations, their appropriate free energies monotonically decay to zero as shown in Fig. 5.

B. Self-similarity and initial conditions

Self-similar structures, as emergent collective phenomena, have been studied in mesoscale crystals²¹, human-scale social network⁶⁰, and the astronomical-scale universe⁶¹. In some models⁶¹, the self-similarity comes from *scale-free* initial conditions with a power-law spectrum^{62,63}. In our CDD model, our simulations start from a random plastic distortion with a Gaussian distribution characterized by a single length scale. The scale-free dislocation structure spontaneously emerges as a result of the deterministic dynamics.

Our Gaussian random initial condition is analogous to hitting a bulk material randomly with a hammer. The hammer head (the dent size scale) corresponds to the correlated length. We need to generate inhomogeneous deformations like random dents, because our theory is deterministic and hence uniform initial conditions under uniform loading will not develop patterns. An alternative to Gaussian random initial conditions might be sinusoidal ones (natural under our periodic boundary conditions).

In our simulations, we mimic a dent in terms of a Gaussian random field with the length scale comparable to the system size L . In fact, at our correlation length scale of $0.28L$, the Gaussian random conditions are nearly sinusoidal (with random phases between components), as discussed in Appendix D 2. As an alternative to inhomogeneous initial conditions, we could have explored inhomogeneous loading — bending our crystals sinusoidally in time, rather than watching the relaxation of an initial bend. We expect this would yield essentially the same fractal structures we study here.

We can introduce multiple small dents in our simulations, by reducing the Gaussian correlation length, as shown in Fig. 6. We find that the initial-scale deformation determines the maximal cutoff for the fractal correlations in our model. In other systems (such as two-dimensional turbulence) one can observe an ‘inverse cascade’ with fractal structures propagating to long length scales; we observe no evidence of these here.

In real materials, initial grain boundaries, impurities, or sample sizes, can be viewed as analogies to our initial dents — explaining the observation of dislocation cellular structures both in single crystals and polycrystalline materials.

Figure 6 shows relaxation without dislocation climb (due to the constraint of a mobile dislocation population) at various initial length scales in 2D. From Fig. 6(a) to (f), the net GND density, the net plastic distortion, and the crystalline orientation map, measured at two well-relaxed states evolved from different random distortions, all show fuzzy fractal structures, distinguished only by their longest-length-scale features that originate from the initial conditions. In Fig. 6(g), (h), and (i), the correlation functions of the GND density ρ , the intrinsic plastic distortion $\beta^{p,1}$, and the crystalline orientation \mathbf{A} are applied to characterize the emergent self-similarity, as discussed in the following section III C. They all exhibit

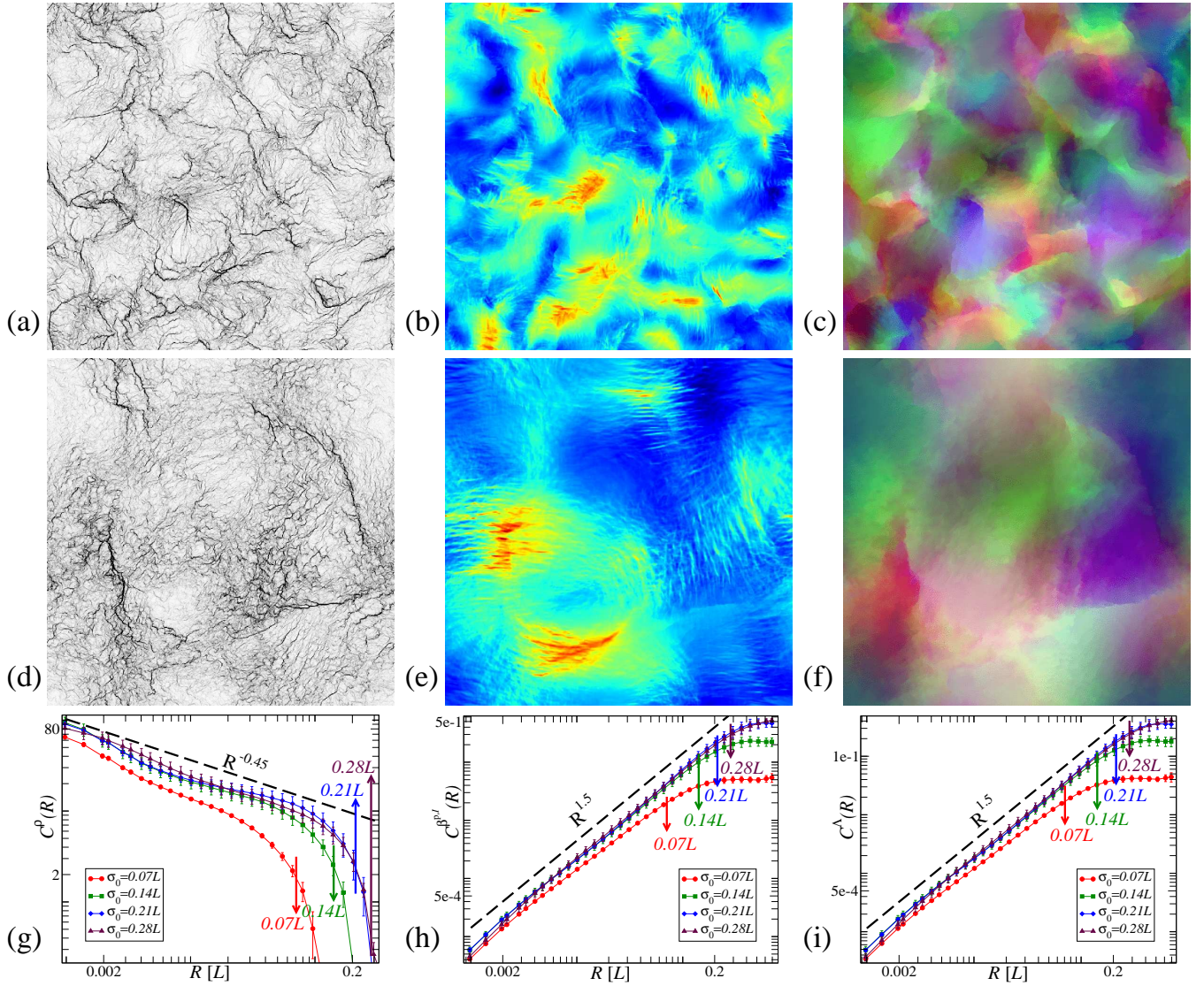


FIG. 6: (Color online) **Relaxation with various initial length scales in two dimensions.** GNDs are not allowed to climb due to the constraint of a mobile dislocation population in these simulations. (a), (b), and (c) are the net GND density map $|\rho|$, the net plastic distortion $|\beta^P|$ (the warmer color indicating the larger distortion), and the crystalline orientation map in a fully-relaxed state evolved from an initial random plastic distortion with correlated length scale $0.07L$. They are compared to the same sequence of plots, (d), (e), and (f), which are in the relaxed state with the initial length scale $0.21L$ three times as long. Notice the features with the longest wave length reflecting the initial distortion length scales. (g), (h), and (i) are the scalar forms (discussed in Sec. III C) of correlation functions of the GND density ρ , the intrinsic plastic distortion β^P , and the crystalline orientation Λ for well-relaxed states with initial length scales varying from $0.07L$ to $0.28L$. They exhibit power laws independent of the initial length scales, with cutoffs set by the initial lengths. (The scaling relation among their critical exponents will be discussed in Sec. IV.)

the same power law, albeit with different cutoffs due to the initial conditions.

C. Correlation functions

Hierarchical dislocation structures have been observed both experimentally¹⁻⁴ and in our simulations²¹. Early work analyzed experimental cellular structures using the fractal box counting method⁷ or by separating the sys-

tems into cells and analyzing their sizes and misorientations²⁶⁻²⁹. In our previous publication, we analyzed our simulated dislocation patterns using these two methods, and showed broad agreement with these experimental analyses²¹. In fact, lack of the measurements of physical order parameters leads to incomplete characterization on the emergent self-similarity⁶⁴. We will not pursue these methods here.

In our view, the emergent self-similarity should best be exhibited by the correlation functions of the order

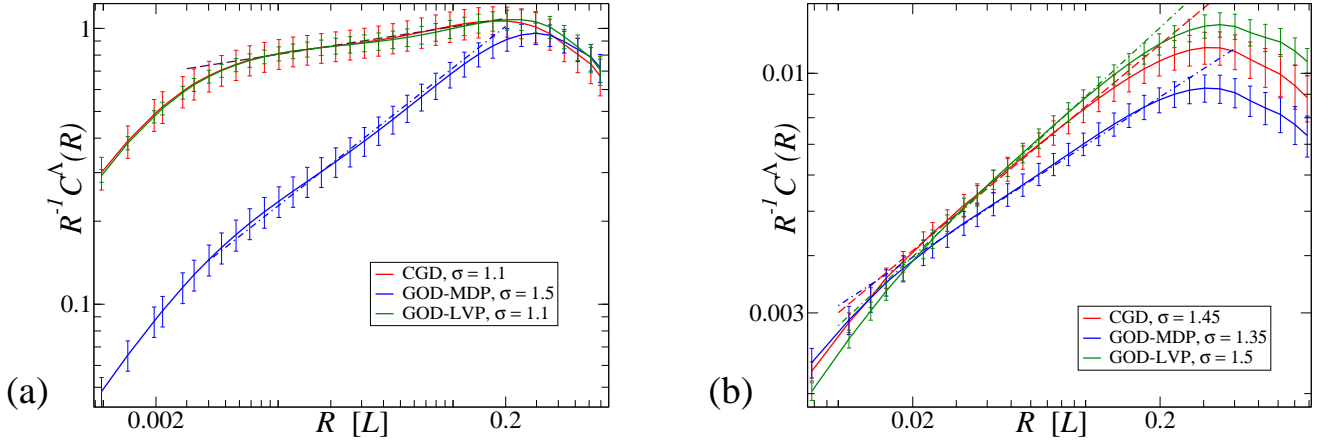


FIG. 7: (Color online) **Correlation functions of Λ in both two and three dimensions.** In (a) and (b), red, blue, and green lines indicate CGD, GOD-MDP, and GOD-LVP simulations, respectively. *Left:* Correlation functions of Λ are measured in relaxed, unstrained 1024^2 systems; *Right:* These correlation functions are measured in relaxed, unstrained 128^3 systems. All dashed lines show estimated power laws quoted in Table I.

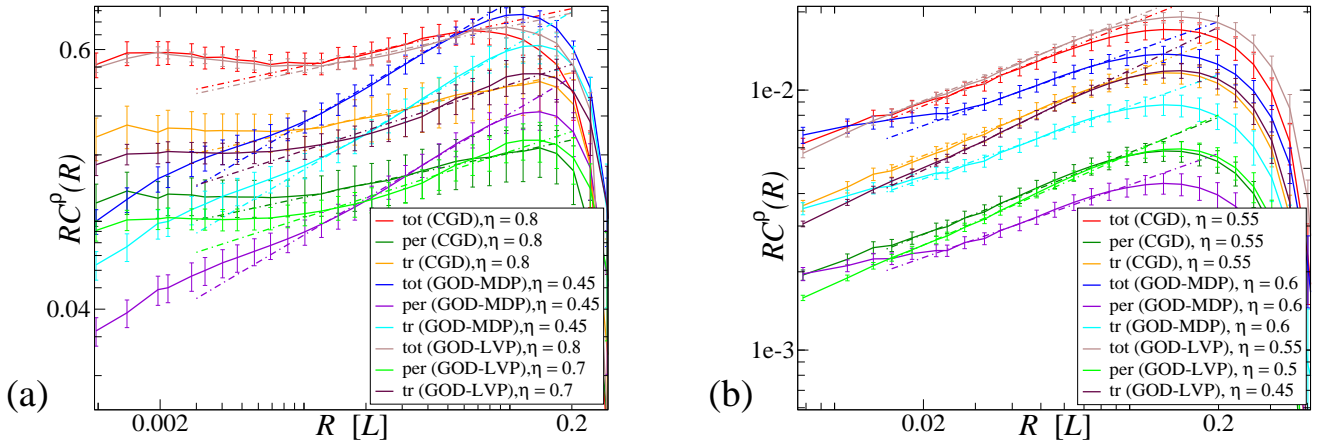


FIG. 8: (Color online) **Correlation functions of ρ in both two and three dimensions.** *Left:* (a) is measured in relaxed, unstrained 1024^2 systems; *Right:* (b) is measured in relaxed, unstrained 128^3 systems. All dashed lines show estimated power laws quoted in Table I. Notice all three scalar forms of the correlation functions of GND density share the same power law.

parameter fields, such as the GND density ρ , the plastic distortion β^P , and the crystalline orientation vector Λ . Here we focus on scalar invariants of the various tensor correlation functions.

For the vector correlation function $C_{ij}^\Lambda(\mathbf{x})$ (Eq. 46), only the sum $C_{ii}^\Lambda(\mathbf{x})$ is a scalar invariant under three dimensional rotations. For the tensor fields ρ and β^P , their two-point correlation functions are measured in terms of a complete set of three independent scalar invariants, which are indicated by ‘tot’ (total), ‘per’ (permutation), and ‘tr’ (trace). In searching for the explanation of the lack of scaling²¹ for β^P (see Sec. III C 3 and Appendix E1), we checked whether these independent invariants might scale independently. In fact, most of them share a single underlying critical exponent, except for the trace-type scalar invariant of the correlation function of β^P ,¹ which go to a constant in well-relaxed states, as discussed in Sec. IV A 2.

1. Correlation function of crystalline orientation field

As dislocations self-organize themselves into complex structures, the relative differences of the crystalline orientations are correlated over a long length scale.

For a vector field, like the crystalline orientation Λ , the natural two-point correlation function is

$$\begin{aligned} C_{ij}^\Lambda(\mathbf{x}) &= \langle (\Lambda_i(\mathbf{x}) - \Lambda_i(0))(\Lambda_j(\mathbf{x}) - \Lambda_j(0)) \rangle \\ &= 2\langle \Lambda_i \Lambda_j \rangle - 2\langle \Lambda_i(\mathbf{x}) \Lambda_j(0) \rangle. \end{aligned} \quad (46)$$

Note that we correlate changes in Λ between two points. Just as for the height-height correlation function in surface growth³⁴, adding a constant to $\Lambda(\mathbf{x})$ (rotating the sample) leads to an equivalent configuration, so only differences in rotations can be meaningfully correlated.

It can be also described in Fourier space

$$\tilde{\mathcal{C}}_{ij}^{\Lambda}(\mathbf{k}) = 2\langle\Lambda_i\Lambda_j\rangle(2\pi)^3\delta(\mathbf{k}) - \frac{2}{V}\tilde{\Lambda}_i(\mathbf{k})\tilde{\Lambda}_j(-\mathbf{k}). \quad (47)$$

In an isotropic medium, we study the scalar invariant formed from $\mathcal{C}_{ij}^{\Lambda}$

$$\mathcal{C}^{\Lambda}(\mathbf{x}) = \mathcal{C}_{ii}^{\Lambda}(\mathbf{x}) = 2\langle\Lambda^2\rangle - 2\langle\Lambda_i(\mathbf{x})\Lambda_i(0)\rangle. \quad (48)$$

Figure 7 shows the correlation functions of crystalline orientations in both 1024^2 and 128^3 simulations. The large shift in critical exponents seen in 2D (Fig. 7(a)) for both CGD and GOD-LVP is not observed in the fully three dimensional simulations (Fig. 7(b)).

2. Correlation function of GND density field

As GNDs evolve into δ -shock singularities, the critical fluctuations of the GND density can be measured by the two-point correlation function $\mathcal{C}^{\rho}(\mathbf{x})$ of the GND density, which decays as the separating distance between two sites increases. The complete set of rotational invariants of the correlation function of ρ includes three scalar forms

$$\mathcal{C}_{tot}^{\rho}(\mathbf{x}) = \langle\rho_{ij}(\mathbf{x})\rho_{ij}(0)\rangle, \quad (49)$$

$$\mathcal{C}_{per}^{\rho}(\mathbf{x}) = \langle\rho_{ij}(\mathbf{x})\rho_{ji}(0)\rangle, \quad (50)$$

$$\mathcal{C}_{tr}^{\rho}(\mathbf{x}) = \langle\rho_{ii}(\mathbf{x})\rho_{jj}(0)\rangle. \quad (51)$$

Figure 8 shows all the correlation functions of GND density in both 1024^2 and 128^3 simulations. These three scalar forms of the correlation functions of ρ exhibit the same critical exponent η , as listed in Table I. Similar to the measurements of \mathcal{C}^{Λ} , the large shift in critical exponents seen in 2D (Fig. 8(a)) for both CGD and GOD-LVP

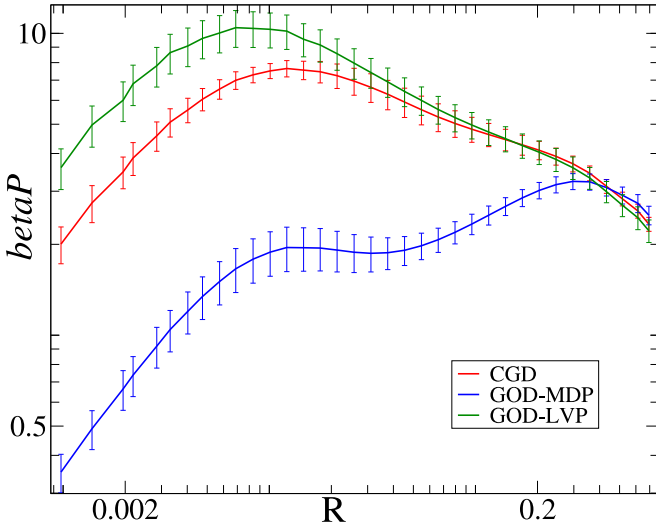


FIG. 9: (Color online) **Correlation functions of β^P in two dimensions.** Red, blue, and green lines indicate CGD, GOD-MDP, and GOD-LVP simulations, respectively. None of these curves shows a convincing power law.

is not observed in the fully three dimensional simulations (Fig. 8(b)).

3. Correlation function of plastic distortion field

The plastic distortion β^P is a mixture of both the divergence-free $\beta^{P,I}$ and the curl-free $\beta^{P,H}$. Figure 9 shows that β^P does not appear to be scale invariant, as observed in our earlier work²¹. It is crucial to study the correlations of the two physical fields, $\beta^{P,I}$ and $\beta^{P,H}$, separately.

Similarly to the crystalline orientation Λ , we correlate the differences between $\beta^{P,I}$ at neighboring points. The complete set of scalar invariants of correlation functions of $\beta^{P,I}$ thus includes the three scalar forms

$$\begin{aligned} \mathcal{C}_{tot}^{\beta^{P,I}}(\mathbf{x}) &= \langle(\beta_{ij}^{P,I}(\mathbf{x}) - \beta_{ij}^{P,I}(0))(\beta_{ij}^{P,I}(\mathbf{x}) - \beta_{ij}^{P,I}(0))\rangle \\ &= 2\langle\beta_{ij}^{P,I}\beta_{ij}^{P,I}\rangle - 2\langle\beta_{ij}^{P,I}(\mathbf{x})\beta_{ij}^{P,I}(0)\rangle; \end{aligned} \quad (52)$$

$$\begin{aligned} \mathcal{C}_{per}^{\beta^{P,I}}(\mathbf{x}) &= -\langle(\beta_{ij}^{P,I}(\mathbf{x}) - \beta_{ij}^{P,I}(0))(\beta_{ji}^{P,I}(\mathbf{x}) - \beta_{ji}^{P,I}(0))\rangle \\ &= -2\langle\beta_{ij}^{P,I}\beta_{ji}^{P,I}\rangle + 2\langle\beta_{ij}^{P,I}(\mathbf{x})\beta_{ji}^{P,I}(0)\rangle; \end{aligned} \quad (53)$$

$$\begin{aligned} \mathcal{C}_{tr}^{\beta^{P,I}}(\mathbf{x}) &= \langle(\beta_{ii}^{P,I}(\mathbf{x}) - \beta_{ii}^{P,I}(0))(\beta_{jj}^{P,I}(\mathbf{x}) - \beta_{jj}^{P,I}(0))\rangle \\ &= 2\langle\beta_{ii}^{P,I}\beta_{jj}^{P,I}\rangle - 2\langle\beta_{ii}^{P,I}(\mathbf{x})\beta_{jj}^{P,I}(0)\rangle; \end{aligned} \quad (54)$$

where an overall minus sign is added to $\mathcal{C}_{per}^{\beta^{P,I}}$ so as to yield a positive measure.

In Fig. 10, the correlation functions of the intrinsic plastic distortion $\beta^{P,I}$ in both 1024^2 and 128^3 simulations exhibit a critical exponent σ' . These measured critical exponents are shown in Table I. We discuss the less physically relevant case of $\beta^{P,H}$ in Appendix E 1, Fig. 15.

IV. SCALING THEORY

The emergent self-similar dislocation morphologies are characterized by the rotational invariants of correlation functions of physical observables, such as the GND density ρ , the crystalline orientation Λ , and the intrinsic plastic distortion $\beta^{P,I}$. Here we derive the relations expected between these correlation functions, and show that their critical exponents collapse into a single underlying one through a generic scaling theory.

In our model, the initial elastic stresses are relaxed via dislocation motion, leading to the formation of cellular structures. In the limit of slow imposed deformations, the elastic stress goes to zero in our model. We will use the absence of external stress to simplify our correlation function relations. (Some relations can be valid regardless of the existence of residual stress.) Those relations that hold only in stress-free states will be labeled ‘sf’; they will be applicable in analyzing experiments only insofar as residual stresses are small.

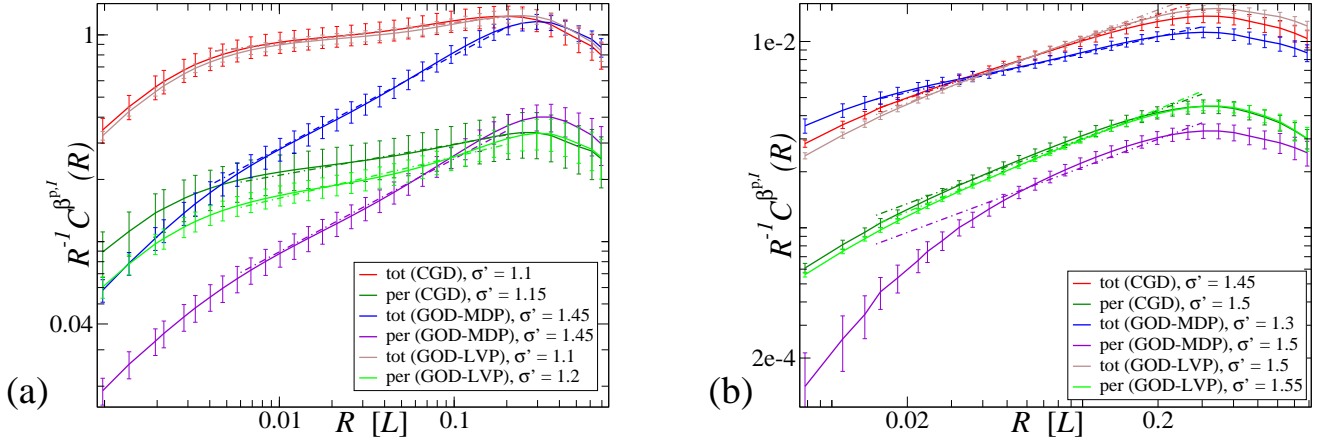


FIG. 10: (Color online) **Correlation functions of $\beta^{p,1}$ in both two and three dimensions.** In (a) and (b), the correlation functions of the intrinsic part of plastic distortion field are shown. *Left:* (a) is measured in relaxed, unstrained 1024^2 systems; *Right:* (b) is measured in relaxed, unstrained 128^3 systems. All dashed lines show estimated power laws quoted in Table I. Notice that we omit the correlation functions of $C_{tr}^{\beta^{p,1}}$, which are independent of distance, and unrelated to the emergent self-similarity, as shown in Sec. IV A 2.

A. Relations between correlation functions

1. C^ρ and C^Λ

For a stress-free state, we thus ignore the elastic strain term in Eq. (14) and write in Fourier space

$$\tilde{\rho}_{ij}(\mathbf{k}) \stackrel{\text{sf}}{=} -ik_j \tilde{\Lambda}_i(\mathbf{k}) + i\delta_{ij} k_k \tilde{\Lambda}_k(\mathbf{k}). \quad (55)$$

First, we can substitute Eq. (55) into the Fourier-transformed form of the correlation function Eq. (49)

$$\begin{aligned} \tilde{C}_{tot}^\rho(\mathbf{k}) &\stackrel{\text{sf}}{=} \frac{1}{V} \left(-ik_j \tilde{\Lambda}_i(\mathbf{k}) + i\delta_{ij} k_k \tilde{\Lambda}_k(\mathbf{k}) \right) \\ &\quad \times \left(ik_j \tilde{\Lambda}_i(-\mathbf{k}) - i\delta_{ij} k_m \tilde{\Lambda}_m(-\mathbf{k}) \right) \\ &\stackrel{\text{sf}}{=} \frac{1}{V} (\delta_{ij} k^2 + k_i k_j) \tilde{\Lambda}_i(\mathbf{k}) \tilde{\Lambda}_j(-\mathbf{k}). \end{aligned} \quad (56)$$

Multiplying both sides of Eq. (47) by $(\delta_{ij} k^2 + k_i k_j)$ gives

$$(\delta_{ij} k^2 + k_i k_j) \tilde{C}_{ij}^\Lambda(\mathbf{k}) \stackrel{\text{sf}}{=} -\frac{2}{V} (\delta_{ij} k^2 + k_i k_j) \tilde{\Lambda}_i(\mathbf{k}) \tilde{\Lambda}_j(-\mathbf{k}). \quad (57)$$

Comparing Eq. (57) and Eq. (56), we may write \tilde{C}_{tot}^ρ in terms of \tilde{C}_{ij}^Λ as

$$\tilde{C}_{tot}^\rho(\mathbf{k}) \stackrel{\text{sf}}{=} -\frac{1}{2} (\delta_{ij} k^2 + k_i k_j) \tilde{C}_{ij}^\Lambda(\mathbf{k}). \quad (58)$$

Second, we can substitute Eq. (55) into the Fourier-transformed form of the correlation function Eq. (50)

$$\tilde{C}_{per}^\rho(\mathbf{k}) \stackrel{\text{sf}}{=} \frac{2}{V} k_i k_j \tilde{\Lambda}_i(\mathbf{k}) \tilde{\Lambda}_j(-\mathbf{k}). \quad (59)$$

Multiplying both sides of Eq. (47) by $k_i k_j$ and comparing with Eq. (59) gives

$$\tilde{C}_{per}^\rho(\mathbf{k}) \stackrel{\text{sf}}{=} -k_i k_j \tilde{C}_{ij}^\Lambda(\mathbf{k}). \quad (60)$$

Finally, we substitute Eq. (55) into the Fourier-transformed form of the correlation function Eq. (51)

$$\tilde{C}_{tr}^\rho(\mathbf{k}) \stackrel{\text{sf}}{=} \frac{4}{V} k_i k_j \tilde{\Lambda}_i(\mathbf{k}) \tilde{\Lambda}_j(-\mathbf{k}). \quad (61)$$

Repeating the same procedure of deriving \tilde{C}_{per}^ρ , we write \tilde{C}_{tr}^ρ in terms of \tilde{C}_{ij}^Λ as

$$\tilde{C}_{tr}^\rho(\mathbf{k}) \stackrel{\text{sf}}{=} -2k_i k_j \tilde{C}_{ij}^\Lambda(\mathbf{k}). \quad (62)$$

Through an inverse Fourier transform, we convert Eq. (58), Eq. (60), and Eq. (62) back to real space to find

$$C_{tot}^\rho(\mathbf{x}) \stackrel{\text{sf}}{=} \frac{1}{2} \partial^2 C^\Lambda(\mathbf{x}) + \frac{1}{2} \partial_i \partial_j C_{ij}^\Lambda(\mathbf{x}), \quad (63)$$

$$C_{per}^\rho(\mathbf{x}) \stackrel{\text{sf}}{=} \partial_i \partial_j C_{ij}^\Lambda(\mathbf{x}), \quad (64)$$

$$C_{tr}^\rho(\mathbf{x}) \stackrel{\text{sf}}{=} 2\partial_i \partial_j C_{ij}^\Lambda(\mathbf{x}). \quad (65)$$

2. $C^{\beta^{p,1}}$ and C^Λ

The intrinsic part of the plastic distortion field is directly related to the GND density field. In stress-free states, the crystalline orientation vector can fully describe the GND density. We thus can connect $C^{\beta^{p,1}}$ to C^Λ .

First, substituting $\tilde{\beta}_{ij}^{p,I} = -i\varepsilon_{ilm}k_l\tilde{\rho}_{mj}/k^2$ into the Fourier-transformed form of Eq. (52) gives

$$\begin{aligned}\tilde{\mathcal{C}}_{tot}^{\beta^{p,1}}(\mathbf{k}) &= 2\langle\beta_{ij}^{p,I}\beta_{ij}^{p,I}\rangle(2\pi)^3\delta(\mathbf{k}) - \frac{2}{V}\left(-i\varepsilon_{ilm}\frac{k_l}{k^2}\tilde{\rho}_{mj}(\mathbf{k})\right) \\ &\quad \times \left(i\varepsilon_{ist}\frac{k_s}{k^2}\tilde{\rho}_{tj}(-\mathbf{k})\right) \\ &= 2\langle\beta_{ij}^{p,I}\beta_{ij}^{p,I}\rangle(2\pi)^3\delta(\mathbf{k}) - \frac{2}{k^2}\left(\frac{1}{V}\tilde{\rho}_{mj}(\mathbf{k})\tilde{\rho}_{mj}(-\mathbf{k})\right).\end{aligned}\quad (66)$$

During this derivation, some terms vanish due to the geometrical constraint on ρ , Eq. (6). Multiplying $-k^2/2$ on both sides of Eq. (66) and applying the Fourier-transformed form of Eq. (49) gives

$$-\frac{k^2}{2}\tilde{\mathcal{C}}_{tot}^{\beta^{p,1}}(\mathbf{k}) = \tilde{\mathcal{C}}_{tot}^{\rho}(\mathbf{k}). \quad (67)$$

In stress-free states, we can substitute Eq. (58) into Eq. (67)

$$-\frac{k^2}{2}\tilde{\mathcal{C}}_{tot}^{\beta^{p,1}}(\mathbf{k}) \stackrel{\text{sf}}{=} \tilde{\mathcal{C}}_{tot}^{\rho, \text{sf}}(\mathbf{k}) = -\frac{1}{2}\left(\delta_{ij}k^2 + k_ik_j\right)\tilde{\mathcal{C}}_{ij}^{\Lambda}(\mathbf{k}), \quad (68)$$

which is rewritten after multiplying $-2/k^2$ on both sides

$$\tilde{\mathcal{C}}_{tot}^{\beta^{p,1}}(\mathbf{k}) \stackrel{\text{sf}}{=} \tilde{\mathcal{C}}^{\Lambda}(\mathbf{k}) + \frac{k_ik_j}{k^2}\tilde{\mathcal{C}}_{ij}^{\Lambda}(\mathbf{k}). \quad (69)$$

Second, substituting $\tilde{\beta}_{ij}^{p,I} = -i\varepsilon_{ilm}k_l\tilde{\rho}_{mj}/k^2$ into the Fourier-transformed form of Eq. (53) gives

$$\begin{aligned}\tilde{\mathcal{C}}_{per}^{\beta^{p,1}}(\mathbf{k}) &= -2\langle\beta_{ij}^{p,I}\beta_{ji}^{p,I}\rangle(2\pi)^3\delta(\mathbf{k}) + \frac{2}{V}\left(-i\varepsilon_{ilm}\frac{k_l}{k^2}\tilde{\rho}_{mj}(\mathbf{k})\right) \\ &\quad \times \left(i\varepsilon_{jst}\frac{k_s}{k^2}\tilde{\rho}_{ti}(-\mathbf{k})\right) \\ &= -2\langle\beta_{ij}^{p,I}\beta_{ji}^{p,I}\rangle(2\pi)^3\delta(\mathbf{k}) + \frac{2}{k^2}\tilde{\mathcal{C}}_{tot}^{\rho}(\mathbf{k}) \\ &\quad - \frac{2}{k^2}\tilde{\mathcal{C}}_{tr}^{\rho}(\mathbf{k}) - \frac{2}{Vk^4}k_ik_j\tilde{\rho}_{mj}(\mathbf{k})\tilde{\rho}_{mi}(-\mathbf{k}),\end{aligned}\quad (70)$$

where we skip straightforward but tedious expansions and the geometrical constraint on ρ , Eq. (6). Notice that this relation is correct even in the presence of stress.

In stress-free states, we substitute Eqs. (55), (58), (62) into Eq. (70), and ignore the constant zero wavelength term

$$\begin{aligned}\tilde{\mathcal{C}}_{per}^{\beta^{p,1}}(\mathbf{k}) &\stackrel{\text{sf}}{=} -\frac{1}{k^2}(k^2\delta_{ij} + k_ik_j)\tilde{\mathcal{C}}_{ij}^{\Lambda}(\mathbf{k}) + \frac{4}{k^2}k_ik_j\tilde{\mathcal{C}}_{ij}^{\Lambda}(\mathbf{k}) \\ &\quad - \frac{2k_ik_j}{Vk^4}\left(-ik_j\tilde{\Lambda}_m(\mathbf{k}) + i\delta_{mj}k_k\tilde{\Lambda}_k(\mathbf{k})\right) \\ &\quad \times \left(ik_i\tilde{\Lambda}_m(-\mathbf{k}) - i\delta_{mi}k_n\tilde{\Lambda}_n(-\mathbf{k})\right) \\ &\stackrel{\text{sf}}{=} 2\frac{k_ik_j}{k^2}\tilde{\mathcal{C}}_{ij}^{\Lambda}(\mathbf{k}).\end{aligned}\quad (71)$$

Finally, substituting $\tilde{\beta}_{ij}^{p,I} = -i\varepsilon_{ilm}k_l\tilde{\rho}_{mj}/k^2$ into the Fourier-transformed form of Eq. (54) gives

$$\begin{aligned}\tilde{\mathcal{C}}_{tr}^{\beta^{p,1}}(\mathbf{k}) &= 2\langle\beta_{ii}^{p,I}\beta_{jj}^{p,I}\rangle(2\pi)^3\delta(\mathbf{k}) - \frac{2}{V}\left(-i\varepsilon_{ilm}\frac{k_l}{k^2}\tilde{\rho}_{mi}(\mathbf{k})\right) \\ &\quad \times \left(i\varepsilon_{jst}\frac{k_s}{k^2}\tilde{\rho}_{tj}(-\mathbf{k})\right) \\ &= 2\langle\beta_{ii}^{p,I}\beta_{jj}^{p,I}\rangle(2\pi)^3\delta(\mathbf{k}) - \frac{2}{k^2}\tilde{\mathcal{C}}_{tot}^{\rho}(\mathbf{k}) + \frac{2}{k^2}\tilde{\mathcal{C}}_{per}^{\rho}(\mathbf{k}) \\ &\quad + \frac{2}{Vk^4}k_ik_j\tilde{\rho}_{mi}(\mathbf{k})\tilde{\rho}_{mj}(-\mathbf{k}),\end{aligned}\quad (72)$$

valid in the presence of stress. Here we repeat a similar procedure as was used to derive in Eq. (70).

In stress-free states, we substitute Eqs. (55), (58), (60) into Eq. (72)

$$\begin{aligned}\tilde{\mathcal{C}}_{tr}^{\beta^{p,1}}(\mathbf{k}) &\stackrel{\text{sf}}{=} 2\langle\beta_{ii}^{p,I}\beta_{jj}^{p,I}\rangle(2\pi)^3\delta(\mathbf{k}) \\ &\quad + \frac{1}{k^2}(k^2\delta_{ij} + k_ik_j)\tilde{\mathcal{C}}_{ij}^{\Lambda}(\mathbf{k}) - \frac{2}{k^2}k_ik_j\tilde{\mathcal{C}}_{ij}^{\Lambda}(\mathbf{k}) \\ &\quad + \frac{2k_ik_j}{Vk^4}\left(-ik_i\tilde{\Lambda}_m(\mathbf{k}) + i\delta_{mi}k_k\tilde{\Lambda}_k(\mathbf{k})\right) \\ &\quad \times \left(ik_j\tilde{\Lambda}_m(-\mathbf{k}) - i\delta_{mj}k_n\tilde{\Lambda}_n(-\mathbf{k})\right) \\ &\stackrel{\text{sf}}{=} 2\langle\beta_{ii}^{p,I}\beta_{jj}^{p,I}\rangle(2\pi)^3\delta(\mathbf{k}),\end{aligned}\quad (73)$$

which is a trivial constant in space.

Through an inverse Fourier transform, Eqs. (69), (71), and (73) can be converted back to real space, giving

$$\mathcal{C}_{tot}^{\beta^{p,1}}(\mathbf{x}) \stackrel{\text{sf}}{=} \mathcal{C}^{\Lambda}(\mathbf{x}) + \frac{1}{4\pi}\int d^3\mathbf{x}'\left(\frac{\delta_{ij}}{R^3} - 3\frac{R_iR_j}{R^5}\right)\mathcal{C}_{ij}^{\Lambda}(\mathbf{x}'), \quad (74)$$

$$\mathcal{C}_{per}^{\beta^{p,1}}(\mathbf{x}) \stackrel{\text{sf}}{=} \frac{1}{2\pi}\int d^3\mathbf{x}'\left(\frac{\delta_{ij}}{R^3} - 3\frac{R_iR_j}{R^5}\right)\mathcal{C}_{ij}^{\Lambda}(\mathbf{x}'), \quad (75)$$

$$\mathcal{C}_{tr}^{\beta^{p,1}}(\mathbf{x}) \stackrel{\text{sf}}{=} 2\int d^3\mathbf{x}'\beta_{ii}^{p,I}(\mathbf{x}')\beta_{jj}^{p,I}(\mathbf{x}') = 2\langle\beta_{ii}^{p,I}\beta_{jj}^{p,I}\rangle, \quad (76)$$

where $\mathbf{R} = \mathbf{x}' - \mathbf{x}$. According to Eqs. (69) and (71), we can extract a relation

$$\mathcal{C}_{per}^{\beta^{p,1}}(\mathbf{x}) - 2\mathcal{C}_{tot}^{\beta^{p,1}}(\mathbf{x}) + 2\mathcal{C}^{\Lambda}(\mathbf{x}) \stackrel{\text{sf}}{=} \text{const.} \quad (77)$$

We can convert Eq. (67) through an inverse Fourier transform

$$\mathcal{C}_{tot}^{\rho}(\mathbf{x}) = \frac{1}{2}\partial^2\mathcal{C}_{tot}^{\beta^{p,1}}(\mathbf{x}), \quad (78)$$

or

$$\mathcal{C}_{tot}^{\beta^{p,1}}(\mathbf{x}) = -\frac{1}{2\pi}\int d^3\mathbf{x}'\frac{\mathcal{C}_{tot}^{\rho}(\mathbf{x}')}{R}, \quad (79)$$

valid in the presence of residual stress.

TABLE I: Critical exponents for correlation functions at stress-free states.

Correlation functions	Scaling theory	Simulations					
		Climb&Glide		Glide Only (MDP)		LVP Glide Only (LVP)	
		2D(1024 ²)	3D(128 ³)	2D(1024 ²)	3D(128 ³)	2D(1024 ²)	3D(128 ³)
\mathcal{C}_{tot}^ρ	η	0.80 ± 0.30	0.55 ± 0.05	0.45 ± 0.25	0.60 ± 0.20	0.80 ± 0.30	0.55 ± 0.05
\mathcal{C}_{per}^ρ	η	0.80 ± 0.20	0.55 ± 0.05	0.45 ± 0.20	0.60 ± 0.20	0.70 ± 0.30	0.50 ± 0.05
\mathcal{C}_{tr}^ρ	η	0.80 ± 0.20	0.55 ± 0.05	0.45 ± 0.20	0.60 ± 0.10	0.70 ± 0.30	0.45 ± 0.05
\mathcal{C}^Λ	$2 - \eta$	1.10 ± 0.65	1.45 ± 0.25	1.50 ± 0.30	1.35 ± 0.25	1.10 ± 0.65	1.50 ± 0.25
$\mathcal{C}_{tot}^{\beta^{p,1}}$	$2 - \eta$	1.10 ± 0.60	1.45 ± 0.15	1.45 ± 0.25	1.30 ± 0.20	1.10 ± 0.60	1.50 ± 0.20
$\mathcal{C}_{per}^{\beta^{p,1}}$	$2 - \eta$	1.15 ± 0.45	1.50 ± 0.25	1.45 ± 0.25	1.50 ± 0.50	1.20 ± 0.45	1.55 ± 0.25

B. Critical exponent relations

When the self-similar dislocation structures emerge, the correlation functions of all physical quantities are expected to exhibit scale-free power laws. We consider the simplest possible scenario, where single variable scaling is present to reveal the minimal number of underlying critical exponents.

First, we define the critical exponent η as the power law describing the asymptotic decay of $\mathcal{C}_{tot}^\rho(\mathbf{x}) \sim |\mathbf{x}|^{-\eta}$, one of the correlation functions for the GND density tensor (summed over components). If we rescale the spatial variable \mathbf{x} by a factor b , the correlation function \mathcal{C}^ρ is rescaled by the power law as

$$\mathcal{C}_{tot}^\rho(b\mathbf{x}) = b^{-\eta} \mathcal{C}_{tot}^\rho(\mathbf{x}). \quad (80)$$

Similarly, the correlation function of the crystalline orientation field Λ is described by a power law, $\mathcal{C}^\Lambda(\mathbf{x}) \sim |\mathbf{x}|^\sigma$, where σ is its critical exponent. We repeat the rescaling by the same factor b

$$\mathcal{C}^\Lambda(b\mathbf{x}) = b^\sigma \mathcal{C}^\Lambda(\mathbf{x}). \quad (81)$$

Since \mathcal{C}_{tot}^ρ can be written in terms of \mathcal{C}^Λ , Eq. (63), we rescale this relation by the same factor b

$$\mathcal{C}_{tot}^\rho(b\mathbf{x}) \stackrel{\text{sf}}{=} \frac{1}{2} \left[\frac{\partial}{b} \right]^2 \mathcal{C}^\Lambda(b\mathbf{x}) + \frac{1}{2} \left[\frac{\partial_i}{b} \right] \left[\frac{\partial_j}{b} \right] \mathcal{C}_{ij}^\Lambda(b\mathbf{x}). \quad (82)$$

Substituting Eq. (81) into Eq. (82) gives

$$\begin{aligned} \mathcal{C}_{tot}^\rho(b\mathbf{x}) &\stackrel{\text{sf}}{=} b^{\sigma-2} \left[\frac{1}{2} \partial^2 \mathcal{C}^\Lambda(\mathbf{x}) + \frac{1}{2} \partial_i \partial_j \mathcal{C}_{ij}^\Lambda(\mathbf{x}) \right] \\ &\stackrel{\text{sf}}{=} b^{\sigma-2} \mathcal{C}_{tot}^\rho(\mathbf{x}). \end{aligned} \quad (83)$$

Comparing with Eq. (80) gives a relation between σ and η

$$\sigma = 2 - \eta. \quad (84)$$

We can repeat the same renormalization group procedure to analyze the critical exponents of the other two scalar forms of the correlation functions of the GND density field. Clearly, \mathcal{C}_{per}^ρ and \mathcal{C}_{tr}^ρ share the same critical exponent η with \mathcal{C}_{tot}^ρ .

Also, we can define the critical exponent σ' as the power law describing the asymptotic growth of $\mathcal{C}_{tot}^{\beta^{p,1}}(\mathbf{x}) \sim |\mathbf{x}|^{\sigma'}$, one of the correlation functions for the intrinsic part of the plastic distortion field. We can rescale the correlation function $\mathcal{C}^{\beta^{p,1}}$

$$\mathcal{C}_{tot}^{\beta^{p,1}}(b\mathbf{x}) = b^{\sigma'} \mathcal{C}_{tot}^{\beta^{p,1}}(\mathbf{x}). \quad (85)$$

We rescale the relation Eq. (78) by the same factor b , and substitute Eq. (85) into it

$$\begin{aligned} \mathcal{C}_{tot}^\rho(b\mathbf{x}) &= \frac{1}{2} \left[\frac{\partial}{b} \right]^2 \mathcal{C}_{tot}^{\beta^{p,1}}(b\mathbf{x}) = b^{\sigma'-2} \left[\frac{1}{2} \partial^2 \mathcal{C}_{tot}^{\beta^{p,1}}(\mathbf{x}) \right] \\ &= b^{\sigma'-2} \mathcal{C}_{tot}^\rho(\mathbf{x}). \end{aligned} \quad (86)$$

Comparing with Eq. (80) also gives a relation between σ' and η

$$\sigma' = 2 - \eta. \quad (87)$$

Since both $\mathcal{C}_{tot}^{\beta^{p,1}}$ and \mathcal{C}^Λ share the same critical exponent $2 - \eta$, it is clear that $\mathcal{C}_{per}^{\beta^{p,1}}$, the other scalar form of the correlation functions of the intrinsic plastic distortion field, also shares this critical exponent, according to Eq. (77).

Thus the correlation functions of three physical quantities (the GND density ρ , the crystalline orientation Λ , and the intrinsic plastic distortion $\beta^{p,1}$) all share the same underlying universal critical exponent η for self-similar morphologies, in the case of zero residual stress, and still hold in the limit of slow imposed deformation. Table I verifies the existence of single underlying critical exponent in both two and three dimensional simulations for each type of dynamics. Imposed strain, studied in Ref. 21, could in principle change η , but the scaling relations derived here should still apply. The strain, of course, breaks the isotropic symmetry, allowing even more allowed correlation functions to be measured.

V. CONCLUSION

In our earlier works^{21,24,36}, we have proposed a flexible framework of CDD to study complex mesoscale phenom-

ena of collective dislocation motion. Traditionally, deterministic CDDs have missed the experimentally ubiquitous feature of cellular pattern formation. Our CDD models have made progress in that respect. In the beginning, we focused our efforts on describing coarse-grained dislocations that naturally develop dislocation cellular structures in ways that are consistent with experimental observations of scale invariance and fractality, a target achieved in Ref. 21. However, that paper studied only 2D, instead of the more realistic 3D.

In this manuscript, we go further in many aspects of the theory extending the results of our previous work:

We provide a derivation of our theory that explains the differences with traditional theories of plasticity. In addition to our previously studied climb-glide (CGD) and glide-only (GOD-MDP) models, we extend our construction in order to incorporate vacancies, and re-derive⁴² a different glide-only dynamics (GOD-LVP) which we show exhibits very similar behavior in 2D to our CGD model. It is worth mentioning that in this way, the GOD-LVP and the CGD dynamics become statistically similar in 2D, while the previously studied, less physical, GOD-MDP model provides rather different behavior in 2D²¹.

We present 3D simulation results here for the first time, showing qualitatively different behavior from that of 2D. In 3D, all three types of dynamics – CGD, GOD-MDP and GOD-LVP – show similar non-trivial fractal patterns and scaling dimensions. Thus our 3D analysis shows that the flatter ‘grain boundaries’ we observe in the 2D simulations are not intrinsic to our dynamics, but are an artifact of the artificial z -independent initial conditions. Experimentally, grain boundaries are indeed flatter and cleaner than cell walls, and our theory no longer provides a new explanation for this distinction. We expect that the dislocation core energies left out of our model would flatten the walls, and that adding disorder or entanglement would prevent the low-temperature glide-only dynamics from flattening as much.

We also fully describe, in a statistical sense, multiple correlation functions – the local orientation, the plastic distortion, the GND density – their symmetries and their mutual scaling relations. Correlation functions of important physical quantities are categorized and analytically shown to share one stress-free exponent. The anomaly in the correlation functions of β^p , which was left as a question in our previous publication²¹, has been discussed and explained. All of these correlation functions and properties are verified with the numerical results of the dynamics that we extensively discussed.

As discussed in Sec. I, our model is an immensely simplified caricature of the deformation of real materials. How does it connect to reality?

First, we show that a model for which elastic strain energy minimization determines the dynamics produces realistic cell wall structures even while ignoring slip systems, crystalline anisotropy²⁷, pinning, junction formation, and statistically stored dislocations. The fact that low-energy dislocation structures (LEDS) provides natu-

ral explanations for many properties of these structures has long been emphasized by Kuhlmann-Wilsdorf⁶⁵. Intermittent flow, forest interactions, and pinning will in general impede access to low energy states. These real-world features, our model suggests, can be important for the morphology of the cell wall structures but are not the root cause of their formation nor of their evolution under stress (discussed in previous work²¹).

One must note, however, that strain energy minimization does not provide the explanation for wall structures in our model material. Indeed, there is an immense space of dislocation densities which make the strain energy zero⁴⁵, including many continuous densities. Our dynamics relaxes into a small subset of these allowed structures – it is the dynamics that leads to cell structure formation here, not purely the energy. In discrete dislocation simulations and real materials, the quantization of the Burger’s vector leads to a weak logarithmic energetic preference for sharp walls. This $-\mu\mathbf{b}/(4\pi(1-\nu))\theta \log \theta$ energy of low-angle grain boundaries yields a $\log 2$ preference for one wall of angle θ rather than two walls of angle $\theta/2$. This leads to a ‘zipping’ together of low angle grain boundaries. Since $\mathbf{b} \rightarrow 0$ in a continuum theory, this preference is missing from our model. Yet, we still find cell wall formation suggesting that such mechanisms are not central to cell wall formation.

Second, how should we connect our fractal cell wall structures with those (fractal or non-fractal) seen in experiments? Many qualitatively different kinds of cellular structures are seen in experiments – variously termed cell block structures, mosaic structures, ordinary cellular structures, . . . Hansen et al.³¹ recently categorized these structures into three types, and argue that the orientation of the stress with respect to the crystalline axes largely determines which morphology is exhibited. The cellular structures in our model, which ignores crystalline anisotropy, likely are the theoretical progenitors of all of these morphologies. In particular, Hansen’s type 1 and type 3 structures incorporate both ‘geometrically necessary’ and ‘incidental dislocation’ boundaries (GNBs and IDBs), while type 2 structures incorporate only the latter. Our simulations cannot distinguish between these two types, and indeed qualitatively look similar to Hansen’s type 2 structures. One should note that the names of these boundaries are misleading – the ‘incidental’ boundaries do mediate geometrical rotations, with the type 2 boundaries at a given strain having similar average misorientations to the geometrically necessary boundaries of type 1 structures (Ref. 31, Fig. 8). It is commonly asserted that the IDBs are formed by statistical trapping of stored dislocations; our model suggests that stochasticity is not necessary for their formation.

Third, how is our model compatible with traditional plasticity, which focuses on the total density of dislocation lines? Our model evolves the net dislocation density, ignoring the *geometrically unnecessary* or *statistically stored* dislocations with canceling Burger’s vectors. These latter dislocations are important for yield stress

and work hardening on macroscales, but are invisible to our theory (since they do not generate stress). Insofar as the cancellation of Burger's vectors on the macroscale is due to cell walls of opposing misorientations on the mesoscale, there needs to be no conflict here. Also our model remains agnostic about whether cell boundaries include significant components of geometrically unnecessary dislocations. However, our model does assume that the driving force for cell boundary formation is the motion of geometrically necessary dislocations, as opposed to (for example) inhomogeneous flows of statistically stored dislocations.

There still remain many fascinating mesoscale experiments, such as dislocation avalanches^{66,67}, size-dependent hardness (smaller is stronger)⁶⁸, and complex anisotropic loading^{69,70}, that we hope to emulate. We intend in the future to include several relevant additional ingredients to our dynamics, such as vacancies (Appendix C 1), impurities (Appendix C 2), immobile dislocations/SSDs and slip systems, to reflect real materials.

Acknowledgments

We would like to thank A. Alemi, P. Dawson, R. LeVaque, M. Miller, E. Siggia, A. Vladimirovsky, D. Warner, M. Zaiser and S. Zapperi for helpful and inspiring discussions on plasticity and numerical methods over the last three years. We were supported by the Basic Energy Sciences (BES) program of DOE through DE-FG02-07ER46393. Our work was partially supported by the National Center for Supercomputing Applications under MSS090037 and utilized the Lincoln and Abe clusters.

Appendix A: Physical quantities in terms of the plastic distortion tensor β^p

In an isotropic infinitely large medium, the local deformation \mathbf{u} , the elastic distortion β^e and the internal long-range stress σ^{int} can be expressed^{24,71} in terms of

the plastic distortion field β^p in Fourier space:

$$\begin{aligned}\tilde{\mathbf{u}}_i(\mathbf{k}) &= N_{ikl}(\mathbf{k})\tilde{\beta}_{kl}^p(\mathbf{k}), \\ N_{ikl}(\mathbf{k}) &= -\frac{i}{k^2}(k_k\delta_{il} + k_l\delta_{ik}) - i\frac{\nu k_i\delta_{kl}}{(1-\nu)k^2} \\ &\quad + i\frac{k_ik_kk_l}{(1-\nu)k^4};\end{aligned}\tag{A1}$$

$$\begin{aligned}\tilde{\beta}_{ij}^e(\mathbf{k}) &= T_{ijkl}(\mathbf{k})\tilde{\beta}_{kl}^p(\mathbf{k}), \\ T_{ijkl}(\mathbf{k}) &= \frac{1}{k^2}(k_ik_k\delta_{jl} + k_ik_l\delta_{jk} - k^2\delta_{ik}\delta_{jl}) \\ &\quad + \frac{k_ik_j}{(1-\nu)k^4}(\nu k^2\delta_{kl} - k_kk_l);\end{aligned}\tag{A2}$$

$$\begin{aligned}\tilde{\sigma}_{ij}^{\text{int}}(\mathbf{k}) &= M_{ijmn}(\mathbf{k})\tilde{\beta}_{mn}^p(\mathbf{k}), \\ M_{ijmn}(\mathbf{k}) &= \frac{2u\nu}{1-\nu}\left(\frac{k_mk_n\delta_{ij} + k_ik_j\delta_{mn}}{k^2} - \delta_{ij}\delta_{mn}\right) \\ &\quad + u\left(\frac{k_ik_m}{k^2}\delta_{jn} + \frac{k_jk_n}{k^2}\delta_{im} - \delta_{im}\delta_{jn}\right) \\ &\quad + u\left(\frac{k_ik_n}{k^2}\delta_{jm} + \frac{k_jk_m}{k^2}\delta_{in} - \delta_{in}\delta_{jm}\right) \\ &\quad - \frac{2u}{1-\nu}\frac{k_ik_jk_mk_n}{k^4}.\end{aligned}\tag{A3}$$

All these expressions are valid for systems with periodic boundary conditions.

According to the definition Eq. (12) of the crystalline orientation Λ , we can replace ω^e with β^e and ϵ^e by using the elastic distortion tensor decomposition Eq. (10)

$$\Lambda_i = \frac{1}{2}\varepsilon_{ijk}(\beta_{jk}^e - \epsilon_{jk}^e).\tag{A4}$$

Here the permutation factor acting on the symmetric elastic strain tensor gives zero. Hence we can express the crystalline orientation vector Λ in terms of β^p by using Eq. (A2)

$$\begin{aligned}\tilde{\Lambda}_i(\mathbf{k}) &= \frac{1}{2}\varepsilon_{ijk}\left\{\frac{1}{k^2}(k_jk_s\delta_{kt} + k_jk_t\delta_{ks} - k^2\delta_{js}\delta_{kt})\right. \\ &\quad \left. + \frac{k_jk_k}{(1-\nu)k^4}(\nu k^2\delta_{st} - k_s k_t)\right\}\tilde{\beta}_{st}^p(\mathbf{k}) \\ &= \frac{1}{2k^2}(\varepsilon_{ijt}k_jk_s + \varepsilon_{ijs}k_jk_t - k^2\varepsilon_{ist})\tilde{\beta}_{st}^p(\mathbf{k}).\end{aligned}\tag{A5}$$

Appendix B: Energy dissipation rate

1. Free energy in Fourier space

In the absence of external stress, the free energy \mathcal{F} is the elastic energy caused by the internal long-range stress

$$\mathcal{F} = \int d^3\mathbf{x} \frac{1}{2}\sigma_{ij}^{\text{int}}\epsilon_{ij}^e = \int d^3\mathbf{x} \frac{1}{2}C_{ijmn}\epsilon_{ij}^e\epsilon_{mn}^e,\tag{B1}$$

where the stress is $\sigma_{ij}^{\text{int}} = C_{ijmn}\epsilon_{mn}^e$, with C_{ijmn} the stiffness tensor.

Using the symmetry of C_{ijmn} and ignoring large rotations, $\epsilon_{ij}^e = (\beta_{ij}^e + \beta_{ji}^e)/2$, we can rewrite the elastic energy \mathcal{F} in terms of β^e

$$\mathcal{F} = \int d^3\mathbf{x} \frac{1}{2} C_{ijmn} \beta_{ij}^e \beta_{mn}^e. \quad (\text{B2})$$

Performing a Fourier transform on both β_{ij}^p and β_{mn}^p simultaneously gives

$$\begin{aligned} \mathcal{F} &= \int d^3\mathbf{x} \int \frac{d^3\mathbf{k}}{(2\pi)^3} \int \frac{d^3\mathbf{k}'}{(2\pi)^3} e^{i(\mathbf{k}+\mathbf{k}')\mathbf{x}} \\ &\times \left(\frac{1}{2} C_{ijmn} \tilde{\beta}_{ij}^e(\mathbf{k}) \tilde{\beta}_{mn}^e(\mathbf{k}') \right). \end{aligned} \quad (\text{B3})$$

Integrating out the spatial variable \mathbf{x} leaves a δ -function $\delta(\mathbf{k}+\mathbf{k}')$ in Eq. (B3). We hence integrate out the k-space variable \mathbf{k}'

$$\mathcal{F} = \int \frac{d^3\mathbf{k}}{(2\pi)^3} \frac{1}{2} C_{ijmn} \tilde{\beta}_{ij}^e(\mathbf{k}) \tilde{\beta}_{mn}^e(-\mathbf{k}). \quad (\text{B4})$$

Substituting Eq. (A2) into Eq. (B4) gives

$$\begin{aligned} \mathcal{F} &= \int \frac{d^3\mathbf{k}}{(2\pi)^3} \frac{1}{2} (C_{ijmn} T_{ijpq}(\mathbf{k}) T_{mnst}(-\mathbf{k})) \tilde{\beta}_{pq}^p(\mathbf{k}) \tilde{\beta}_{st}^p(-\mathbf{k}) \\ &= - \int \frac{d^3\mathbf{k}}{(2\pi)^3} \frac{1}{2} M_{pqst}(\mathbf{k}) \tilde{\beta}_{pq}^p(\mathbf{k}) \tilde{\beta}_{st}^p(-\mathbf{k}), \end{aligned} \quad (\text{B5})$$

where we skip straightforward but tedious simplifications.

When turning on the external stress, we repeat the same procedure used in Eq. (B3), yielding

$$\mathcal{F}^{\text{ext}} = - \int d^3\mathbf{x} \sigma_{ij}^{\text{ext}} \beta_{ij}^p = - \int \frac{d^3\mathbf{k}}{(2\pi)^3} \tilde{\sigma}_{ij}^{\text{ext}}(\mathbf{k}) \tilde{\beta}_{ij}^p(-\mathbf{k}). \quad (\text{B6})$$

2. Calculation of energy functional derivative with respect to the GND density ϱ

According to Eq. (17), the infinitesimal change of the variable $\delta\varrho$ is given in terms of $\delta\beta^p$

$$\delta\varrho_{ijk} = -g_{ijls} \partial_l (\delta\beta_{sk}^p). \quad (\text{B7})$$

Substituting Eq. (B7) into Eq. (27) and applying integration by parts, the infinitesimal change of \mathcal{F} is hence rewritten in terms of β^p

$$\delta\mathcal{F}[\beta^p] = \int d^3\mathbf{x} g_{ijls} \partial_l \left(\frac{\delta\mathcal{F}}{\delta\varrho_{ijk}} \right) \delta\beta_{sk}^p. \quad (\text{B8})$$

According to Eq. (24), it suggests

$$\delta\mathcal{F}[\beta^p] = \int d^3\mathbf{x} \frac{\delta\mathcal{F}}{\delta\beta_{sk}^p} \delta\beta_{sk}^p = \int d^3\mathbf{x} (-\sigma_{sk}) \delta\beta_{sk}^p. \quad (\text{B9})$$

Comparing Eq. (B8) and Eq. (B9) implies

$$g_{ijls} \partial_l \left(\frac{\delta\mathcal{F}}{\delta\varrho_{ijk}} \right) = -\sigma_{sk}, \quad (\text{B10})$$

up to a total derivative which we ignore due to the use of periodic boundary conditions.

3. Derivation of energy dissipation rate

We can apply variational methods to calculate the dissipation rate of the free energy. As is well known, the general elastic energy \mathcal{E} in a crystal can be expressed as $\mathcal{E} = \frac{1}{2} \int d^3\mathbf{x} \sigma_{ij} \epsilon_{ij}^e$, with ϵ_{ij}^e the elastic strain. An infinitesimal change of \mathcal{E} is:

$$\delta\mathcal{E} = \frac{1}{2} \int d^3\mathbf{x} \sigma_{ij} \delta\epsilon_{ij}^e + \frac{1}{2} \int d^3\mathbf{x} \delta\sigma_{ij} \epsilon_{ij}^e = \int d^3\mathbf{x} \sigma_{ij} \delta\epsilon_{ij}^e, \quad (\text{B11})$$

where we use $\sigma_{ij} \delta\epsilon_{ij}^e = C_{ijkl} \epsilon_{kl}^e \delta\epsilon_{ij}^e = \delta\sigma_{ij} \epsilon_{ij}^e$.

So the infinitesimal change of the free energy Eq. (20) is

$$\delta\mathcal{F} = \int d^3\mathbf{x} \left(\sigma_{ij}^{\text{int}} \delta\epsilon_{ij}^e - \sigma_{ij}^{\text{ext}} \delta\epsilon_{ij}^p \right). \quad (\text{B12})$$

We apply the relation $\epsilon^e = \epsilon - \epsilon^p$, where ϵ^p is the plastic strain and ϵ is the total strain:

$$\delta\mathcal{F} = \int d^3\mathbf{x} \left(\sigma_{ij}^{\text{int}} \delta\epsilon_{ij} - \sigma_{ij}^{\text{int}} \delta\epsilon_{ij}^p - \sigma_{ij}^{\text{ext}} \delta\epsilon_{ij}^p \right). \quad (\text{B13})$$

Using the symmetry of σ_{ij} and ignoring large rotations, $\epsilon_{ij} = \frac{1}{2}(\partial_i u_j + \partial_j u_i)$, we can rewrite the first term of Eq. (B13) as $\int d^3\mathbf{x} \sigma_{ij}^{\text{int}} \delta(\partial_i u_j)$. Integrating by parts yields $\int d^3\mathbf{x} (\partial_i (\delta u_j \sigma_{ij}^{\text{int}}) - \delta u_j \partial_i \sigma_{ij}^{\text{int}})$. We can convert the first volume integral to a surface integral, which vanishes for an infinitely large system. Hence

$$\delta\mathcal{F} = \int d^3\mathbf{x} \left(\partial_i \sigma_{ij}^{\text{int}} \delta u_j - (\sigma_{ij}^{\text{int}} + \sigma_{ij}^{\text{ext}}) \delta\epsilon_{ij}^p \right). \quad (\text{B14})$$

The first term of Eq. (B14) is zero assuming instantaneous elastic relaxation due to the local force equilibrium condition,

$$\delta\mathcal{F} = - \int d^3\mathbf{x} (\sigma_{ij}^{\text{int}} + \sigma_{ij}^{\text{ext}}) \delta\beta_{ij}^p, \quad (\text{B15})$$

using the symmetry of σ_{ij} and $\epsilon_{ij}^p = \frac{1}{2}(\beta_{ij}^p + \beta_{ji}^p)$.

The free energy dissipation rate is thus $\delta\mathcal{F}/\delta t$ or $\delta\beta_{ij}^p = \frac{\partial\beta_{ij}^p}{\partial t} \delta t$, hence

$$\begin{aligned} \frac{\partial\mathcal{F}}{\partial t} &= - \int d^3\mathbf{x} (\sigma_{ij}^{\text{int}} + \sigma_{ij}^{\text{ext}}) \frac{\partial\beta_{ij}^p}{\partial t} \\ &= - \int d^3\mathbf{x} (\sigma_{ij}^{\text{int}} + \sigma_{ij}^{\text{ext}}) J_{ij}. \end{aligned} \quad (\text{B16})$$

When dislocations are allowed to climb, substituting the CGD current Eq. (36) into Eq. (B16) implies that the free energy dissipation rate is strictly negative

$$\begin{aligned}\frac{\partial \mathcal{F}}{\partial t} &= - \int d^3 \mathbf{x} (\sigma_{ij}^{\text{int}} + \sigma_{ij}^{\text{ext}}) [v_l \varrho_{lij}] \\ &= - \int d^3 \mathbf{x} \frac{|\varrho|}{D} v^2 \leq 0.\end{aligned}\quad (\text{B17})$$

When removing dislocation climb by considering the mobile dislocation population, we substitute Eq. (40) into Eq. (B16) to guarantee that the rate of the change of the free energy density is also the negative of a perfect square

$$\begin{aligned}\frac{\partial \mathcal{F}}{\partial t} &= - \int d^3 \mathbf{x} (\sigma_{ij}^{\text{int}} + \sigma_{ij}^{\text{ext}}) \left[v_l' \left(\varrho_{lij} - \frac{1}{3} \delta_{ij} \varrho_{lkk} \right) \right] \\ &= - \int d^3 \mathbf{x} \frac{|\varrho|}{D} v'^2 \leq 0.\end{aligned}\quad (\text{B18})$$

Appendix C: Model Extensions: Adding vacancies and disorder to CDD

1. Coupling vacancy diffusion to CDD

In plastically deformed crystals at low temperature, dislocations usually move only in the glide plane because vacancy diffusion is almost frozen out. When temperature increases, vacancy diffusion leads to dislocation climb out of the glide plane. At intermediate temperatures, slow vacancy diffusion can enable local creep. The resulting dynamics should couple the vacancy and dislocation fields in non-trivial ways. Here we couple the vacancy diffusion to the dislocation motion in our CDD model.

We introduce an order parameter field $c(\mathbf{x})$, indicating the vacancy concentration density at the point \mathbf{x} . The free energy \mathcal{F} is thus expressed

$$\mathcal{F} = \mathcal{F}^{\text{Dis}} + \mathcal{F}^{\text{Vac}} = \int d^3 \mathbf{x} \left(\frac{1}{2} \sigma_{ij} \epsilon_{ij}^e + \frac{1}{2} \alpha (c - c_0)^2 \right), \quad (\text{C1})$$

where α is a positive material parameter related to the vacancy creation energy, and c_0 is the overall equilibrium vacancy concentration density.

Assuming that GNDs share the velocity \mathbf{v} in an infinitesimal volume, we write the current J for GNDs

$$J_{ij} = v_u \varrho_{uij}. \quad (\text{C2})$$

The current trace J_{ii} describes the rate of volume change, which acts as a source and sink of vacancies. The coupling dynamics for vacancies is thus given as

$$\partial_t c = \gamma \nabla^2 c + J_{ii}, \quad (\text{C3})$$

where γ is a positive vacancy diffusion constant.

The infinitesimal change of the free energy \mathcal{F} (Eq. C1) is

$$\delta \mathcal{F} = \int d^3 \mathbf{x} \left(\frac{\delta \mathcal{F}^{\text{Dis}}}{\delta \beta_{ij}^{\text{p}}} \delta \beta_{ij}^{\text{p}} + \frac{\delta \mathcal{F}^{\text{Vac}}}{\delta c} \delta c \right). \quad (\text{C4})$$

We apply Eq. (B15) and $\delta \mathcal{F}^{\text{Vac}} / \delta c = \alpha (c - c_0)$

$$\delta \mathcal{F} = \int d^3 \mathbf{x} \left(-\sigma_{ij} \delta \beta_{ij}^{\text{p}} + \alpha (c - c_0) \delta c \right). \quad (\text{C5})$$

The free energy dissipation rate is thus $\delta \mathcal{F} / \delta t$ for $\delta \beta_{ij}^{\text{p}} = \frac{\partial \beta_{ij}^{\text{p}}}{\partial t} \delta t$ and $\delta c = \frac{\partial c}{\partial t} \delta t$, hence

$$\frac{\partial \mathcal{F}}{\partial t} = - \int d^3 \mathbf{x} \left(\sigma_{ij} \frac{\partial \beta_{ij}^{\text{p}}}{\partial t} - \alpha (c - c_0) \frac{\partial c}{\partial t} \right). \quad (\text{C6})$$

Substituting the current J (Eq. C2) and Eq. (C3) into Eq. (C6) gives

$$\begin{aligned}\frac{\partial \mathcal{F}}{\partial t} &= - \int d^3 \mathbf{x} (\sigma_{ij} (v_u \varrho_{uij}) - \alpha (c - c_0) (\gamma \nabla^2 c + v_u \varrho_{uii})) \\ &= - \int d^3 \mathbf{x} ((\sigma_{ij} - \alpha (c - c_0) \delta_{ij}) \varrho_{uij}) v_u \\ &\quad - \int d^3 \mathbf{x} \alpha \gamma (\nabla c)^2,\end{aligned}\quad (\text{C7})$$

where we integrate by parts by assuming an infinitely large system.

If we choose the velocity $v_u = \frac{D}{|\varrho|} (\sigma_{ij} - \alpha (c - c_0) \delta_{ij}) \varrho_{uij}$, (D is a positive material dependent constant and $1/|\varrho|$ is added for the same reasons as discussed in Sec. II C 1), the free energy is guaranteed to decrease monotonically. The coupling dynamics for both GNDs and vacancies is thus

$$\begin{cases} \partial_t \beta_{ij}^{\text{p}} = \frac{D}{|\varrho|} (\sigma_{mn} - \alpha (c - c_0) \delta_{mn}) \varrho_{umn} \varrho_{uij}, \\ \partial_t c = \gamma \nabla^2 c + \frac{D}{|\varrho|} (\sigma_{mn} - \alpha (c - c_0) \delta_{mn}) \varrho_{umn} \varrho_{ukk}. \end{cases} \quad (\text{C8})$$

This dynamics gives us a clear picture of the underlying physical mechanism: the vacancies contribute an extra hydrostatic pressure $p = -\alpha (c - c_0)$.

2. Coupling disorder to CDD

In real crystals, the presence of precipitates or impurities results in a force pinning nearby dislocations. We can mimic this effect by incorporating a spatially varying random potential field $V(\mathbf{x})$.

In our CDD model, we can add the interaction energy between GNDs and random disorder into the free energy \mathcal{F} (Eq. 20)

$$\mathcal{F} = \mathcal{F}_E + \mathcal{F}_I = \int d^3 \mathbf{x} \left(\frac{1}{2} \sigma_{ij}^{\text{int}} \epsilon_{ij}^e - \sigma_{ij}^{\text{ext}} \epsilon_{ij}^{\text{p}} + V(\mathbf{x}) |\varrho| \right), \quad (\text{C9})$$

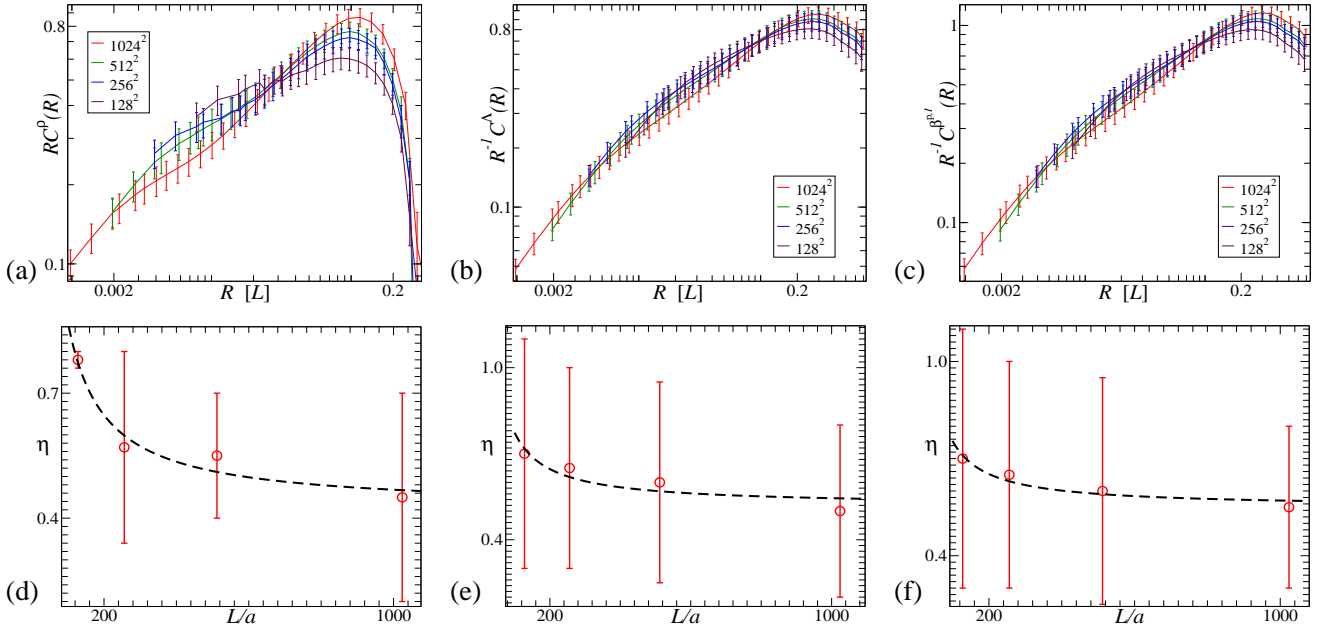


FIG. 11: (Color online) **Statistical convergence of correlation functions of Λ , ρ and $\beta^{p,1}$ by varying lattice sizes in two dimensions.** We compare correlation functions of relaxed glide-only states (GOD-MDP) at resolutions from 128^2 to 1024^2 systems. *Top:* We see that the correlation functions in all cases exhibit similar power laws in (a), (b), and (c); *Bottom:* (d), (e), and (f) show a single underlying critical exponent which appears to converge with increasing resolution, where a is the grid spacing. The black dashed lines are guides to the eye.

where \mathcal{F}_E indicates the elastic free energy corresponding to the integral of the first two terms, and \mathcal{F}_I indicates the interaction energy, the integral of the last term.

An infinitesimal change of the free energy is written

$$\delta\mathcal{F} = \delta\mathcal{F}_E + \delta\mathcal{F}_I = \int d^3\mathbf{x} \left(\frac{\delta\mathcal{F}_E}{\delta\beta_{ij}^p} \delta\beta_{ij}^p + \frac{\delta\mathcal{F}_I}{\delta\beta_{sk}^p} \delta\beta_{sk}^p \right). \quad (\text{C10})$$

In an infinitely large system, Eq. (B15) gives

$$\frac{\delta\mathcal{F}_E}{\delta\beta_{ij}^p} = -(\sigma_{ij}^{\text{int}} + \sigma_{ij}^{\text{ext}}), \quad (\text{C11})$$

and Eq. (B8) implies

$$\begin{aligned} \delta\mathcal{F}_I &= \int d^3\mathbf{x} g_{ijls} \partial_l \left(\frac{\delta\mathcal{F}_I}{\delta\varrho_{ijk}} \right) \delta\beta_{sk}^p \\ &= \int d^3\mathbf{x} g_{ijls} \partial_l \left(V(\mathbf{x}) \frac{\varrho_{ijk}}{|\varrho|} \right) \delta\beta_{sk}^p. \end{aligned} \quad (\text{C12})$$

Substituting Eq. (C11) and Eq. (C12) into Eq. (C10) gives

$$\begin{aligned} \delta\mathcal{F} &= - \int d^3\mathbf{x} \left(\sigma_{ij}^{\text{int}} + \sigma_{ij}^{\text{ext}} - g_{mnl} \partial_l \left(V(\mathbf{x}) \frac{\varrho_{mnj}}{|\varrho|} \right) \right) \delta\beta_{ij}^p \\ &= - \int d^3\mathbf{x} \sigma_{ij}^{\text{eff}} \delta\beta_{ij}^p. \end{aligned} \quad (\text{C13})$$

where the effective stress field is $\sigma_{ij}^{\text{eff}} = \sigma_{ij}^{\text{int}} + \sigma_{ij}^{\text{ext}} - g_{mnl} \partial_l \left(V(\mathbf{x}) \frac{\varrho_{mnj}}{|\varrho|} \right)$.

By replacing σ_{ij} with σ_{ij}^{eff} in the equation of motion of either allowing climb (Eq. 36) or removing climb (Eqs. 40 and 44), we achieve the new CDD model that models GNDs interacting with disorder.

Appendix D: Details of the Simulations

1. Finite size effects

Although we suspect that our simulations don't have weak solutions⁵⁹, we can show that these solutions converge statistically. We use two ways to exhibit the statistical convergence.

When we continue to decrease the grid spacing to zero (the continuum limit), we show the statistical convergence of correlation functions of ρ , Λ , and $\beta^{p,1}$, with a slow expected drift of apparent exponents with system size, see Fig. 11.

We can also decrease the initial correlated length scales in a large two dimensional simulation. Since the emergent self-similar structures are always developed below the initial correlated lengths, as discussed in Sec. III B, this is similar to decreasing the system size by reducing the initial correlated lengths. In Fig. 12, the correlation functions of ρ , Λ , and $\beta^{p,1}$ collapse into a single scaling curve, using finite size scaling.

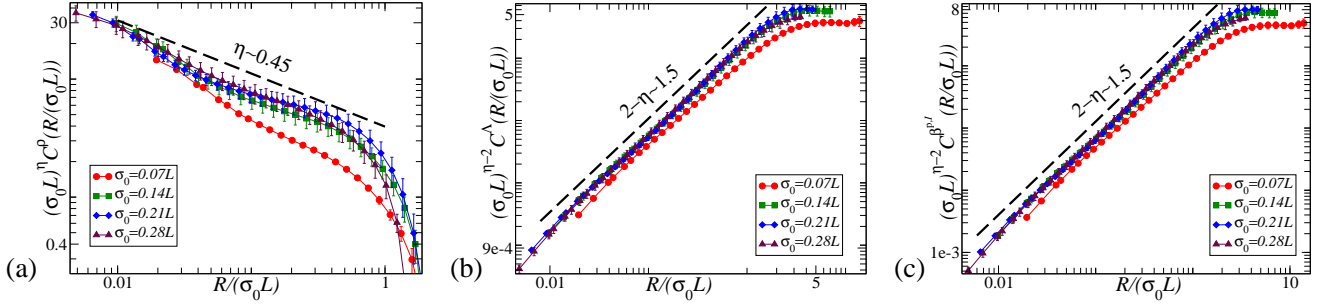


FIG. 12: (Color online) **Statistical convergence of correlation functions of Λ , ρ and $\beta^{p,I}$ by varying the initial length scales in 1024^2 simulations.** We measure correlation functions of relaxed glide-only states (GOD-MDP) at initial correlated lengths from $0.07L$ to $0.28L$. In (a), (b), and (c), the radial-length variable R is rescaled by their initial correlation lengths, and the corresponding correlation functions are divided by the same lengths to the exhibiting powers. They roughly collapse into the scaling laws. Notice that the power laws measured in the state with the initial correlated length $0.07L$ get distorted due to the small outer cutoff.

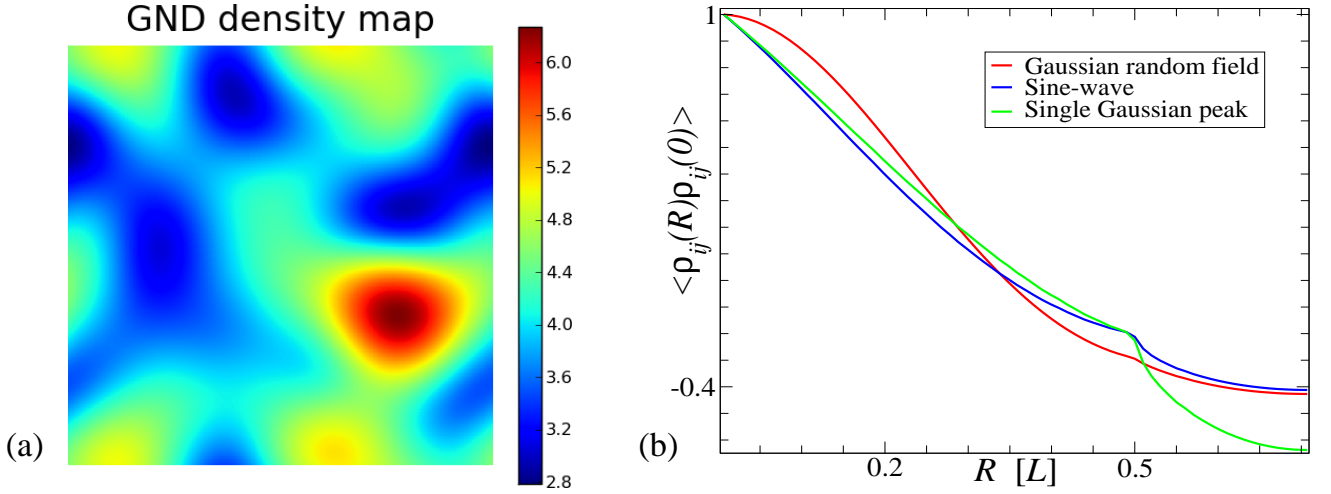


FIG. 13: (Color online) **Gaussian random initial conditions with the correlated length scale $0.28L$ in two dimensions.** (a) shows the initial net GND density map; (b) exhibits the correlation functions of ρ under various initial conditions, where we compare the Gaussian random field to both a sinusoidal wave and a single periodic superposition of Gaussian peaks. The kink arises due to the edges and corners of the square unit cell.

2. Gaussian random initial conditions

Gaussian random fields are extensively used in physical modelings to mimic stochastic fluctuations with a correlated length scale. In our simulations, we construct an initially random plastic distortion, a nine-component tensor field, where every component is an independent Gaussian random field sharing a underlying length scale.

We define a Gaussian random field f with correlation length σ_0 by convolving white noise $\langle \xi(\mathbf{x})\xi(\mathbf{x}') \rangle = \delta(\mathbf{x} - \mathbf{x}')$ with a Gaussian of width σ_0 :

$$f(\mathbf{x}) = \int d^3\mathbf{x}' \xi(\mathbf{x}') e^{-(\mathbf{x}-\mathbf{x}')^2/\sigma_0^2}. \quad (\text{D1})$$

In Fourier space, this can be done as a multiplication:

$$\tilde{f}(\mathbf{k}) = e^{-\sigma_0^2 k^2/4} \tilde{\xi}(\mathbf{k}). \quad (\text{D2})$$

The square $\tilde{f}(\mathbf{k})\tilde{f}(-\mathbf{k}) = e^{-\sigma_0^2 k^2/2}$ implies that the correlation function $\langle f(\mathbf{x})f(\mathbf{x}') \rangle = (2\pi\sigma_0^2)^{-3/2} e^{-(\mathbf{x}-\mathbf{x}')^2/(2\sigma_0^2)}$.

In our simulations, the initial plastic distortion tensor field β^p is constructed in Fourier space

$$\tilde{\beta}_{ij}^p(\mathbf{k}) = e^{-\sigma_0^2 k^2/4} \tilde{\zeta}_{ij}(\mathbf{k}), \quad (\text{D3})$$

where the white noise signal ζ is characterized as $\langle \zeta_{(i,j)}(\mathbf{x})\zeta_{(i,j)}(\mathbf{x}') \rangle = A_{(i,j)}\delta(\mathbf{x} - \mathbf{x}')$, and in Fourier space $\frac{1}{V}\zeta_{(i,j)}(\mathbf{k})\zeta_{(i,j)}(-\mathbf{k}) = A_{(i,j)}$. (We use (i,j) to indicate a component of the tensor field, to avoid the Einstein summation rule.) The correlation function of each component of $\beta^{p,I}$ is thus expressed in Fourier space

$$\begin{aligned} \tilde{C}_{(i,j)}^{\beta^{p,I}} &= 2\langle \beta_{(i,j)}^{p,I}\beta_{(i,j)}^{p,I} \rangle (2\pi)^3 \delta(\mathbf{k}) - \frac{2}{V} \tilde{\beta}_{(i,j)}^p(\mathbf{k}) \tilde{\beta}_{(i,j)}^p(-\mathbf{k}) \\ &= 2\langle \beta_{(i,j)}^{p,I}\beta_{(i,j)}^{p,I} \rangle (2\pi)^3 \delta(\mathbf{k}) - 2A_{(i,j)} e^{-\sigma_0^2 k^2/2}, \end{aligned} \quad (\text{D4})$$

where the Gaussian kernel width σ_0 , as a standard length scale, defines the correlation length of our simulation. (In our earlier work, we use a non-standard definition for the correlation length, so our σ_0 equals the old length scale times $\sqrt{2}$.)

According to Eq. (9) and Eq. (D3), we can express the initial GND density field ρ in Fourier space

$$\tilde{\rho}_{ij}(\mathbf{k}) = -i\varepsilon_{ilm}e^{-\sigma_0^2k^2/4}k_l\tilde{\zeta}_{mj}(\mathbf{k}). \quad (\text{D5})$$

The scalar invariant \mathcal{C}_{tot}^ρ of the correlation function of ρ is thus expressed in Fourier space

$$\begin{aligned} \mathcal{C}_{tot}^\rho(\mathbf{k}) &= \frac{1}{V}\tilde{\rho}_{ij}(\mathbf{k})\tilde{\rho}_{ij}(-\mathbf{k}) \\ &= \frac{1}{V}e^{-\sigma_0^2k^2/2}(k^2\delta_{mn} - k_mk_n)\tilde{\zeta}_{mj}(\mathbf{k})\tilde{\zeta}_{nj}(-\mathbf{k}). \end{aligned} \quad (\text{D6})$$

The resulting initial GND density is not Gaussian correlated, unlike the initial plastic distortion. Figure 13 exhibits the initial GND density map due to the Gaussian random plastic distortions with the correlation length $0.28L$, and its correlation function. We compare the latter to the correlation functions of both a sinusoidal wave and a single periodic superposition of Gaussian peaks. The similarity of the three curves shows that our Gaussian random initial condition at $\sigma_0 \sim 0.28L$ approaches the largest effective correlation length possible for periodic boundary conditions.

Appendix E: Other correlation functions unrelated to static scaling theory

1. Correlation functions of the strain-history-dependent plastic deformation and distortion fields

The curl-free strain-history-dependent part of the plastic distortion field, as shown in Fig. 14(a), (c), and (e), exhibits structures reminiscent of self-similar morphology. We correlate their differences at neighboring points

$$\mathcal{C}_{tot}^{\beta^{\text{p,H}}}(\mathbf{x}) = \langle (\beta_{ij}^{\text{p,H}}(\mathbf{x}) - \beta_{ij}^{\text{p,H}}(0))(\beta_{ij}^{\text{p,H}}(\mathbf{x}) - \beta_{ij}^{\text{p,H}}(0)) \rangle, \quad (\text{E1})$$

$$\mathcal{C}_{per}^{\beta^{\text{p,H}}}(\mathbf{x}) = \langle (\beta_{ij}^{\text{p,H}}(\mathbf{x}) - \beta_{ij}^{\text{p,H}}(0))(\beta_{ji}^{\text{p,H}}(\mathbf{x}) - \beta_{ji}^{\text{p,H}}(0)) \rangle, \quad (\text{E2})$$

$$\mathcal{C}_{tr}^{\beta^{\text{p,H}}}(\mathbf{x}) = \langle (\beta_{ii}^{\text{p,H}}(\mathbf{x}) - \beta_{ii}^{\text{p,H}}(0))(\beta_{jj}^{\text{p,H}}(\mathbf{x}) - \beta_{jj}^{\text{p,H}}(0)) \rangle. \quad (\text{E3})$$

Consider also the deformation field ψ (shown in Fig. 14(b), (d), and (f)) of Eq. (19) whose gradient gives the strain-history-dependent plastic deformation $\beta^{\text{p,H}}$. Similarly to the crystalline orientation $\mathbf{\Lambda}$, we correlate

differences of ψ . The unique rotational invariant of its two-point correlation functions is written

$$\mathcal{C}^\psi(\mathbf{x}) = 2\langle \psi^2 \rangle - 2\langle \psi_i(\mathbf{x})\psi_i(0) \rangle. \quad (\text{E4})$$

In Fig. 15, the correlation functions of the strain-history-dependent plastic distortion $\beta^{\text{p,H}}$ in both 1024^2 and 128^3 simulations show critical exponents τ and τ' . Although apparently unrelated to the previous underlying critical exponent η , this exponents τ and τ' quantify the fractality of the strain-history-dependent plastic distortion. Figure 16 shows the correlation functions of the strain-history-dependent deformation ψ , with the critical exponent τ'' close to 2, which implies a smooth non-fractal field, shown in Fig. 14(c) and (d). All measured critical exponents are listed in Table II.

Figure 15 shows the power-law dependence of the rotational invariants $\mathcal{C}_{per}^{\beta^{\text{p,H}}}$ and $\mathcal{C}_{tr}^{\beta^{\text{p,H}}}$ (they overlap). According to the definition $\tilde{\beta}_{ij}^{\text{p,H}} = ik_i\tilde{\psi}_j$, we can write down the Fourier-transformed forms of Eq. (E2) and Eq. (E3) respectively

$$\tilde{\mathcal{C}}_{per}^{\beta^{\text{p,H}}}(\mathbf{k}) = 2\langle \beta_{ij}^{\text{p,H}}\beta_{ji}^{\text{p,H}} \rangle (2\pi)^3\delta(\mathbf{k}) - \frac{2}{V}k_ik_j\tilde{\psi}_j(\mathbf{k})\tilde{\psi}_i(-\mathbf{k}), \quad (\text{E5})$$

$$\tilde{\mathcal{C}}_{tr}^{\beta^{\text{p,H}}}(\mathbf{k}) = 2\langle \beta_{ii}^{\text{p,H}}\beta_{jj}^{\text{p,H}} \rangle (2\pi)^3\delta(\mathbf{k}) - \frac{2}{V}k_ik_j\tilde{\psi}_i(\mathbf{k})\tilde{\psi}_j(-\mathbf{k}). \quad (\text{E6})$$

Except the zero-wavelength terms, the same functional forms shared by these two rotational scalars explain the observed overlapping power laws.

2. Stress-stress correlation functions

As the system relaxes to its final stress-free state, we can measure the fluctuations of the internal elastic stress fields, using a complete set of two rotational invariants of correlation functions

$$\mathcal{C}_{tot}^\sigma(\mathbf{x}) = \langle \sigma_{ij}^{\text{int}}(\mathbf{x})\sigma_{ij}^{\text{int}}(0) \rangle, \quad (\text{E7})$$

$$\mathcal{C}_{tr}^\sigma(\mathbf{x}) = \langle \sigma_{ii}^{\text{int}}(\mathbf{x})\sigma_{jj}^{\text{int}}(0) \rangle; \quad (\text{E8})$$

and in Fourier space

$$\tilde{\mathcal{C}}_{tot}^\sigma(\mathbf{k}) = \frac{1}{V}\tilde{\sigma}_{ij}^{\text{int}}(\mathbf{k})\tilde{\sigma}_{ij}^{\text{int}}(-\mathbf{k}), \quad (\text{E9})$$

$$\tilde{\mathcal{C}}_{tr}^\sigma(\mathbf{k}) = \frac{1}{V}\tilde{\sigma}_{ii}^{\text{int}}(\mathbf{k})\tilde{\sigma}_{jj}^{\text{int}}(-\mathbf{k}). \quad (\text{E10})$$

Because σ_{ij} is symmetric, these two correlation functions form a complete set of linear invariants under rotational transformations.

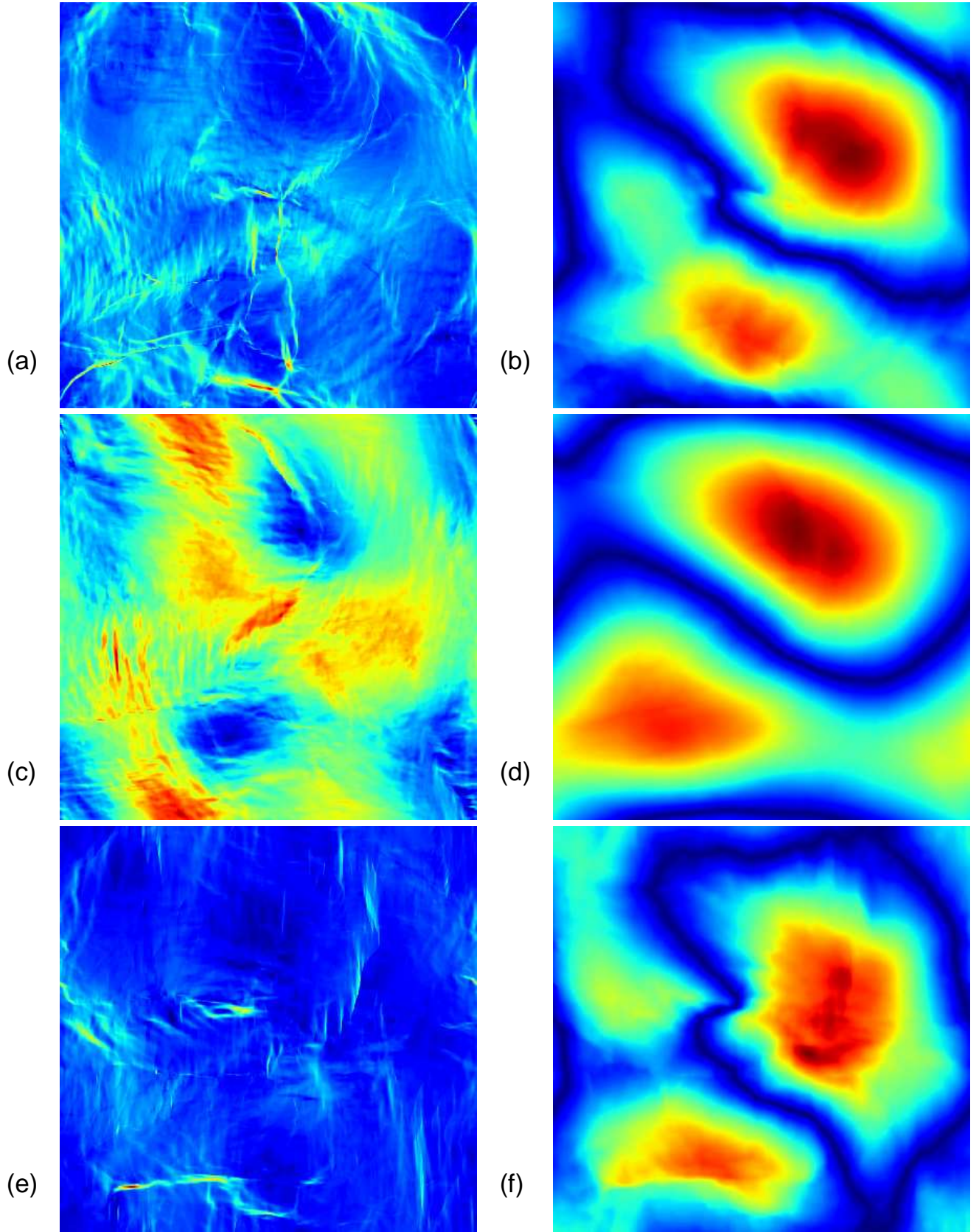


FIG. 14: (Color online) **Strain-history-dependent fields $\beta^{p,H}$ and ψ in two dimensions** for the relaxed states. *Top:* Dislocation climb is allowed; *Middle:* Glide-only using a mobile dislocation population; *Bottom:* Glide-only using a local vacancy pressure. *Left:* The strain-history-dependent plastic distortion $|\beta^{p,H}|$. (a), (c), and (e) exhibit patterns reminiscent of self-similar dislocation structures. *Right:* The strain-history-dependent plastic deformation $|\psi|$. (b), (d), and (f) exhibit smooth patterns with a little distortion, which are not fractal.

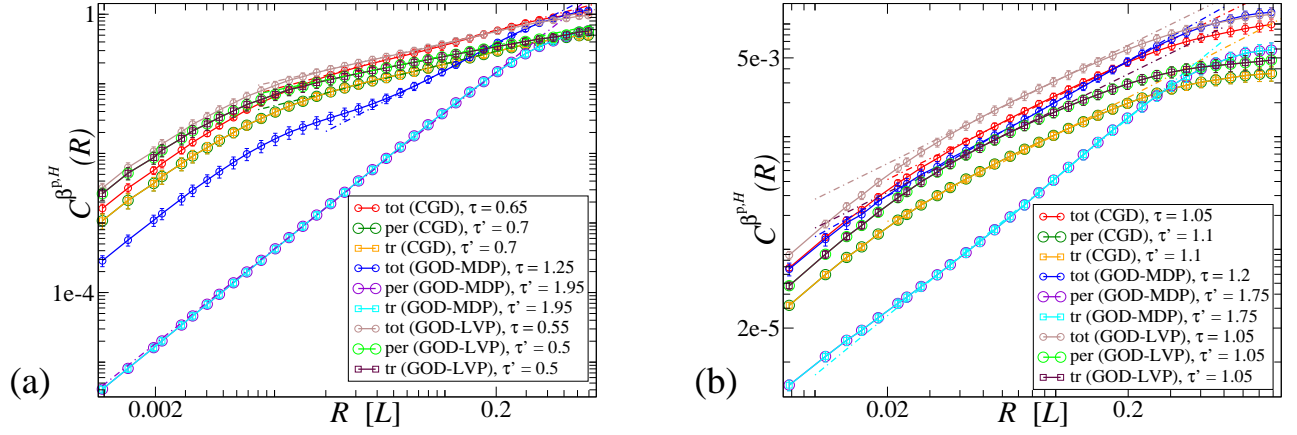


FIG. 15: (Color online) **Correlation functions of $\beta^{p,H}$ in both two and three dimensions.** In both (a) and (b), the correlation functions of the strain-history-dependent part of the plastic distortion $\beta^{p,H}$ are shown. *Left:* (a) is measured in relaxed, unstrained 1024^2 systems; *Right:* (b) is measured in relaxed, unstrained 128^3 systems. All dashed lines show estimated power laws quoted in Table II.

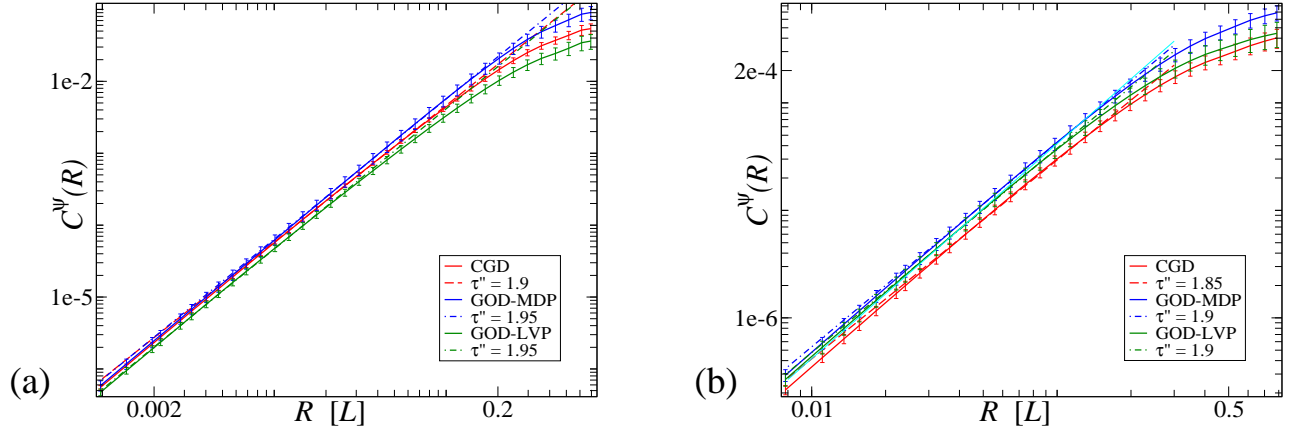


FIG. 16: (Color online) **Correlation functions of ψ in both two and three dimensions.** In (a) and (b), the correlation functions of the strain-history-dependent deformation ψ are shown. Red, blue, green lines indicate CGD, GOD-MDP, and GOD-LVP, respectively. *Left:* (a) is measured in relaxed, unstrained 1024^2 systems; *Right:* (b) is measured in relaxed, unstrained 128^3 systems. All dashed lines show estimated power laws quoted in Table II.

TABLE II: **Critical exponents for correlation functions of strain-history-dependent fields at stress-free states.**

Correlation functions	Exponents	Simulations					
		Climb&Glide		Glide Only (MDP)		Glide Only (LVP)	
		2D(1024^2)	3D(128^3)	2D(1024^2)	3D(128^3)	2D(1024^2)	3D(128^3)
$C_{tot}^{\beta^{p,H}}$	τ	0.65 ± 1.00	1.05 ± 0.65	1.25 ± 0.60	1.20 ± 0.50	0.55 ± 1.10	1.05 ± 0.65
$C_{per}^{\beta^{p,H}}$	τ'	0.70 ± 0.95	1.10 ± 0.60	1.95 ± 0.05	1.75 ± 0.15	0.50 ± 1.15	1.05 ± 0.70
$C_{tr}^{\beta^{p,H}}$	τ'	0.70 ± 0.95	1.10 ± 0.60	1.95 ± 0.05	1.75 ± 0.15	0.50 ± 1.15	1.05 ± 0.70
C^{ψ}	τ''	1.90 ± 0.10	1.85 ± 0.15	1.95 ± 0.05	1.90 ± 0.10	1.95 ± 0.05	1.90 ± 0.10

3. Energy density spectrum

The average internal elastic energy \mathcal{E} is written

$$\begin{aligned} \mathcal{E} &= \frac{1}{V} \int d^d \mathbf{x} \left[\frac{1}{2} \sigma_{ij}^{\text{int}} \epsilon_{ij}^e \right] \\ &= \frac{1}{V} \int d^d \mathbf{x} \frac{1}{4\mu} \left[\sigma_{ij}^{\text{int}} \sigma_{ij}^{\text{int}} - \frac{\nu}{1+\nu} \sigma_{ii}^{\text{int}} \sigma_{jj}^{\text{int}} \right], \end{aligned} \quad (\text{E11})$$

where, in an isotropic bulk medium, the elastic strain ϵ^e is expressed in terms of σ^{int} ,

$$\epsilon_{ij}^e = \frac{1}{2\mu} \left(\sigma_{ij}^{\text{int}} - \frac{\nu}{1+\nu} \delta_{ij} \sigma_{kk}^{\text{int}} \right). \quad (\text{E12})$$

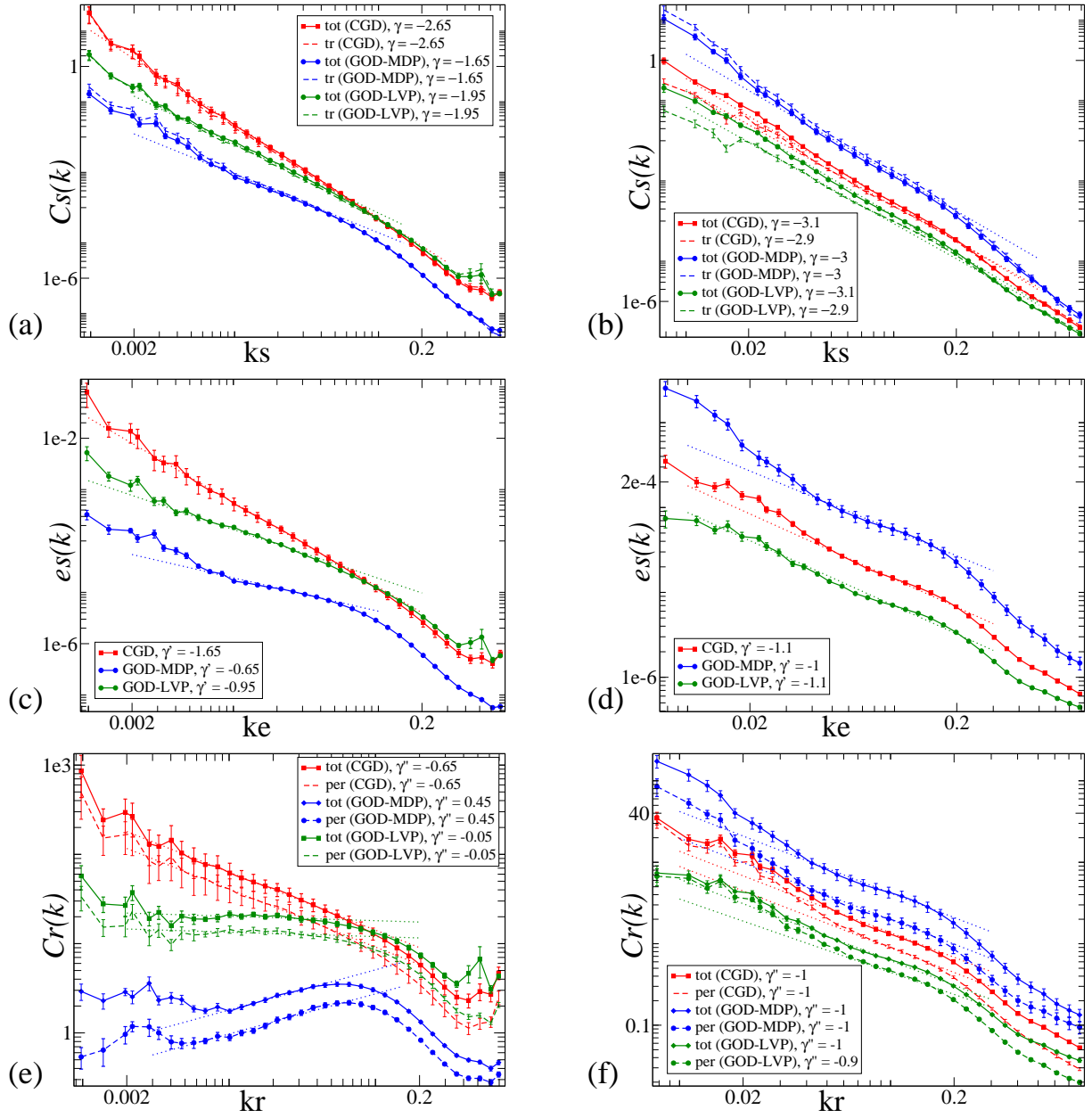


FIG. 17: (Color online) Stress-stress correlation functions $\tilde{C}^\sigma(k)$, elastic energy spectrum $E(k)$, correlation functions of the stressful part of GND density $\tilde{C}^{\rho^E}(k)$. Red, blue, and green lines indicate CGD, GOD-MDP, and GOD-LVP, respectively. All dashed lines show estimated power laws quoted in Table III.

TABLE III: Power-laws relations among $\tilde{C}^\sigma(k)$, $E(k)$, and $\tilde{C}^{\rho^E}(k)$. (d represents the dimension.)

Physical quantities	Scaling Theory	Simulations					
		Climb&Glide		Glide Only (MDP)		Glide Only (LVP)	
		2D(1024 ²)	3D(128 ³)	2D(1024 ²)	3D(128 ³)	2D(1024 ²)	3D(128 ³)
$\tilde{C}_{tot}^\sigma(k)$	γ	-2.65	-3.1	-1.65	-3.0	-1.95	-3.1
$\tilde{C}_{tr}^\sigma(k)$	γ	-2.65	-2.9	-1.65	-3.0	-1.95	-2.9
$E(k)$	$\gamma + d - 1$	-1.65	-1.1	-0.65	-1.0	-0.95	-1.1
$\tilde{C}_{tot}^{\rho^E}(k)$	$\gamma + 2$	-0.65	-1.0	0.45	-1.0	-0.05	-1.0
$\tilde{C}_{per}^{\rho^E}(k)$	$\gamma + 2$	-0.65	-1.0	0.45	-1.0	-0.05	-0.9

We can rewrite Eq. (E11) in Fourier space

$$\mathcal{E} = \frac{1}{V} \int \frac{d^d \mathbf{k}}{(2\pi)^d} \frac{1}{4\mu} \left[\tilde{\sigma}_{ij}^{\text{int}}(\mathbf{k}) \tilde{\sigma}_{ij}^{\text{int}}(-\mathbf{k}) - \frac{\nu}{1+\nu} \tilde{\sigma}_{ii}^{\text{int}}(\mathbf{k}) \tilde{\sigma}_{jj}^{\text{int}}(-\mathbf{k}) \right]. \quad (\text{E13})$$

Substituting Eq. (E9) and Eq. (E10) into Eq. (E13) gives

$$\mathcal{E} = \int \frac{d^d \mathbf{k}}{2^{d+2}\pi^d} \frac{1}{\mu} \left[\tilde{\mathcal{C}}_{\text{tot}}^{\sigma}(\mathbf{k}) - \frac{\nu}{1+\nu} \tilde{\mathcal{C}}_{\text{tr}}^{\sigma}(\mathbf{k}) \right] \quad (\text{E14})$$

If the stress-stress correlation functions are isotropic, we can integrate out the angle variable of Eq. (E14)

$$\mathcal{E} = \int_0^{\infty} dk \frac{f(d)}{\mu} k^{d-1} \left[\tilde{\mathcal{C}}_{\text{tot}}^{\sigma}(k) - \frac{\nu}{1+\nu} \tilde{\mathcal{C}}_{\text{tr}}^{\sigma}(k) \right], \quad (\text{E15})$$

where $f(d)$ is a constant function over the dimension d ,

$$f(d) = \begin{cases} 1/(8\pi) & d = 2, \\ 1/(8\pi^2) & d = 3. \end{cases} \quad (\text{E16})$$

Writing the elastic energy density in terms of the energy density spectrum $\mathcal{E}(t) = \int_0^{\infty} E(k, t) dk$ implies

$$E(k) = \frac{f(d)}{\mu} k^{d-1} \left[\tilde{\mathcal{C}}_{\text{tot}}^{\sigma}(k) - \frac{\nu}{1+\nu} \tilde{\mathcal{C}}_{\text{tr}}^{\sigma}(k) \right]. \quad (\text{E17})$$

4. Correlation function of the stressful part of GND density

According to Eq. (14), the stressful part of GND density is defined as

$$\rho_{ij}^E(\mathbf{x}) = \varepsilon_{isl} \partial_s \epsilon_{lj}^e(\mathbf{x}). \quad (\text{E18})$$

Substituting Eq. (E12) into Eq. (E18) gives

$$\rho_{ij}^E = \frac{1}{2\mu} \varepsilon_{isl} \partial_s \left(\sigma_{lj}^{\text{int}} - \frac{\nu}{1+\nu} \delta_{lj} \sigma_{mm}^{\text{int}} \right). \quad (\text{E19})$$

The complete set of rotational invariants of the correlation function of ρ^E includes three scalar forms

$$\mathcal{C}_{\text{tot}}^{\rho^E}(\mathbf{x}) = \langle \rho_{ij}^E(\mathbf{x}) \rho_{ij}^E(0) \rangle, \quad (\text{E20})$$

$$\mathcal{C}_{\text{per}}^{\rho^E}(\mathbf{x}) = \langle \rho_{ij}^E(\mathbf{x}) \rho_{ji}^E(0) \rangle, \quad (\text{E21})$$

$$\mathcal{C}_{\text{tr}}^{\rho^E}(\mathbf{x}) = \langle \rho_{ii}^E(\mathbf{x}) \rho_{jj}^E(0) \rangle, \quad (\text{E22})$$

where $\mathcal{C}_{\text{tr}}^{\rho^E}(\mathbf{x})$ is always zero due to $\rho_{ii}^E = 0$.

Substituting Eq. (E19) into both Eqs. (E20) and (E21) and applying the Fourier transform gives

$$\begin{aligned} \tilde{\mathcal{C}}_{\text{tot}}^{\rho^E}(\mathbf{k}) &= \frac{1}{4\mu^2 V} \varepsilon_{isl} \varepsilon_{ipq} (ik_s) \left(\tilde{\sigma}_{lj}^{\text{int}}(\mathbf{k}) - \frac{\nu}{1+\nu} \delta_{lj} \tilde{\sigma}_{mm}^{\text{int}}(\mathbf{k}) \right) \varepsilon_{ipq} (-ik_p) \left(\tilde{\sigma}_{qj}^{\text{int}}(-\mathbf{k}) - \frac{\nu}{1+\nu} \delta_{qj} \tilde{\sigma}_{nn}^{\text{int}}(-\mathbf{k}) \right) \\ &= \frac{k^2}{4\mu^2} \left(\frac{1}{V} \tilde{\sigma}_{lj}^{\text{int}}(\mathbf{k}) \tilde{\sigma}_{lj}^{\text{int}}(-\mathbf{k}) \right) - \frac{\nu k^2}{2\mu^2 (1+\nu)^2} \left(\frac{1}{V} \tilde{\sigma}_{mm}^{\text{int}}(\mathbf{k}) \tilde{\sigma}_{nn}^{\text{int}}(-\mathbf{k}) \right), \end{aligned} \quad (\text{E23})$$

$$\begin{aligned} \tilde{\mathcal{C}}_{\text{per}}^{\rho^E}(\mathbf{k}) &= \frac{1}{4\mu^2 V} \varepsilon_{isl} \varepsilon_{ipq} (ik_s) \left(\tilde{\sigma}_{lj}^{\text{int}}(\mathbf{k}) - \frac{\nu}{1+\nu} \delta_{lj} \tilde{\sigma}_{mm}^{\text{int}}(\mathbf{k}) \right) \varepsilon_{jpk} (-ik_p) \left(\tilde{\sigma}_{qi}^{\text{int}}(-\mathbf{k}) - \frac{\nu}{1+\nu} \delta_{qi} \tilde{\sigma}_{nn}^{\text{int}}(-\mathbf{k}) \right) \\ &= \frac{k^2}{4\mu^2} \left(\frac{1}{V} \tilde{\sigma}_{lj}^{\text{int}}(\mathbf{k}) \tilde{\sigma}_{lj}^{\text{int}}(-\mathbf{k}) \right) - \frac{(1+\nu^2)k^2}{4\mu^2 (1+\nu)^2} \left(\frac{1}{V} \tilde{\sigma}_{mm}^{\text{int}}(\mathbf{k}) \tilde{\sigma}_{nn}^{\text{int}}(-\mathbf{k}) \right), \end{aligned} \quad (\text{E24})$$

where we make use of the equilibrium condition $\partial_i \sigma_{ij} = 0$ and thus $k_i \tilde{\sigma}_{ij} = 0$. Substituting Eqs. (E9) and (E10) into Eqs. (E23) and (E24)

$$\tilde{\mathcal{C}}_{\text{tot}}^{\rho^E}(\mathbf{k}) = \frac{k^2}{4\mu^2} \left[\tilde{\mathcal{C}}_{\text{tot}}^{\sigma}(\mathbf{k}) - \frac{2\nu}{(1+\nu)^2} \tilde{\mathcal{C}}_{\text{tr}}^{\sigma}(\mathbf{k}) \right], \quad (\text{E25})$$

$$\tilde{\mathcal{C}}_{\text{per}}^{\rho^E}(\mathbf{k}) = \frac{k^2}{4\mu^2} \left[\tilde{\mathcal{C}}_{\text{tot}}^{\sigma}(\mathbf{k}) - \frac{1+\nu^2}{(1+\nu)^2} \tilde{\mathcal{C}}_{\text{tr}}^{\sigma}(\mathbf{k}) \right]. \quad (\text{E26})$$

Here we can ignore the angle dependence if the stress-stress correlation functions are isotropic.

5. Scaling relations

According to Eq. (E17), the term k^{d-1} suggests that the power-law exponent relation between E and $\tilde{\mathcal{C}}^{\sigma}$ is

$$\gamma' = \gamma + d - 1. \quad (\text{E27})$$

Again, both Eqs. (E23) and (E24) imply that the power-law exponent relation between $\tilde{\mathcal{C}}^{\rho^E}$ and $\tilde{\mathcal{C}}^{\sigma}$ is

$$\gamma'' = \gamma + 2, \quad (\text{E28})$$

regardless of the dimension.

Table III shows a nice agreement between predicted scaling and numerical measurements for power-law exponents of \tilde{C}^σ , E , and \tilde{C}^{ρ^E} . These relations are valid in the presence of residual stress.

During the relaxation processes, the elastic free energy

follows a power-law decay in time asymptotically, seen in Fig. 5. All the above measured correlation functions of elastic quantities share the same power laws in Fourier space, albeit with decaying magnitudes in time.

-
- ¹ Y. Kawasaki and T. Takeuchi, *Scr. Metall.* **14**, 183 (1980).
² H. Mughrabi, T. Ungar, W. Kienle, and M. Wilkens, *Philos. Mag. A* **53**, 793 (1986).
³ C. Schwink, *Scr. Metall. Mater.* **27**, 963 (1992).
⁴ T. Ungár, L. S. Tóth, J. Illy, and I. Kovács, *Acta Metall.* **34**, 1257 (1986).
⁵ J. Gil Sevillano, E. Bouchaud, and L. P. Kubin, *Scr. Metall. Mater.* **25**, 355 (1991).
⁶ J. Gil Sevillano, *Phys. Scr.* **T49B**, 405 (1993).
⁷ P. Hähner, K. Bay, and M. Zaiser, *Phys. Rev. Lett.* **81**, 2470 (1998).
⁸ M. Zaiser, K. Bay, and P. Hähner, *Acta Mater.* **47**, 2463 (1999).
⁹ B. Bakó and I. Groma, *Phys. Rev. B* **60**, 9228 (1999).
¹⁰ B. Bakó, I. Groma, G. Gyorgyi, and G. T. Zimanyi, *Phys. Rev. Lett.* **98**, 075701 (2007).
¹¹ B. Bakó and W. Hoffelner, *Phys. Rev. B* **76**, 214108 (2007).
¹² R. Madec, B. Devincere, and L. P. Kubin, *Scr. Mater.* **47**, 689 (2002).
¹³ D. Gomez-Garcia, B. Devincere, and L. P. Kubin, *Phys. Rev. Lett.* **96**, 125503 (2006).
¹⁴ D. Walgraef and E. Aifantis, *Int. J. Eng. Sci.* **23**, 1351 (1985).
¹⁵ P. Hähner, *Appl. Phys. A* **62**, 473 (1996).
¹⁶ M. Saxlová, J. Kratochvil, and J. Zatloukal, *Mater. Sci. Eng. A* **234**, 205 (1997).
¹⁷ I. Groma and B. Bakó, *Phys. Rev. Lett.* **84**, 1487 (2000).
¹⁸ W. Pantleon, *Scr. Metall.* **35**, 511 (1996).
¹⁹ W. Pantleon, *Acta Mater.* **46**, 451 (1998).
²⁰ J. P. Sethna, V. R. Coffman, and E. Demler, *Phys. Rev. B* **67**, 184107 (2003).
²¹ Y. S. Chen, W. Choi, S. Papanikolaou, and J. P. Sethna, *Phys. Rev. Lett.* **105**, 105501 (2010).
²² A. Acharya, *J. Mech. Phys. Solids* **49**, 761 (2001).
²³ A. Roy and A. Acharya, *J. Mech. Phys. Solids* **53**, 143 (2005).
²⁴ S. Limkumnerd and J. P. Sethna, *Phys. Rev. Lett.* **96**, 095503 (2006).
²⁵ J. F. Nye, *Act. Metall.* **1**, 153 (1953).
²⁶ D. A. Hughes, Q. Liu, D. C. Chrzan, and N. Hansen, *Acta Mater.* **45**, 105 (1997).
²⁷ D. A. Hughes, D. C. Chrzan, Q. Liu, and N. Hansen, *Phys. Rev. Lett.* **81**, 4664 (1998).
²⁸ D. A. Hughes and N. Hansen, *Phys. Rev. Lett.* **87**, 135503 (2001).
²⁹ D. P. Mika and P. R. Dawson, *Acta Mater.* **47**, 1355 (1999).
³⁰ D. Kuhlmann-Wilsdorf, *Metall. Mater. Trans. A* **16**, 2091 (1985).
³¹ N. Hansen, X. Huang, and G. Winther, *Metall. Mater. Trans. A* **42**, 613 (2011).
³² J. A. Wert, X. Huang, G. Winther, W. Pantleon, and H. F. Poulsen, *Materials Today* **10**, 24 (2007).
³³ Y. S. Chen, W. Choi, S. Papanikolaou, and J. P. Sethna, (manuscript in preparation).
³⁴ P. Chaikin and T. Lubensky, *Principles of Condensed Matter Physics* (Cambridge University Press, Cambridge, England, 1995).
³⁵ V. L'vov, *Phys. Rep.* **207**, 1 (1991).
³⁶ W. Choi, Y. S. Chen, S. Papanikolaou, and J. P. Sethna, to be published in *Comput. Sci. Eng.* e-print arXiv:1105.5351.
³⁷ J. P. Sethna, K. A. Dahmen, and C. R. Myers, *Nature* **410**, 242 (2001).
³⁸ Y.S. Chen, W. Choi, S. Papanikolaou, M. Bierbaum, and J.P. Sethna, *Plasticity Tools*, <http://www.lassp.cornell.edu/sethna/Plasticity/Tools/>.
³⁹ L. D. Landau and E. M. Lifshitz, *Theory of Elasticity* (Pergamon Press, 1970), 2nd ed.
⁴⁰ A. Acharya, *Proc. R. Soc. A* **459**, 1343 (2003).
⁴¹ A. Acharya, *J. Mech. Phys. Solids* **52**, 301 (2004).
⁴² A. Acharya and A. Roy, *J. Mech. Phys. Solids* **54**, 1687 (2006).
⁴³ Dislocations which cancel at the macroscale may be geometrically necessary at the mesoscale. The distinction between GND and SSD (statistically stored dislocations, also called geometrically unnecessary dislocations) depends on the coarse-graining length scale. At the mesoscopic scale of dislocation pattern formation, GNDs dominate the dynamics.
⁴⁴ Kröner, in *Physics of Defects, Les Houches, Session XXXV, 1980*, edited by R. Balian, M. Klemann, and J. P. Poirier (North-Holland: Amsterdam, 1981), pp. 215–315.
⁴⁵ S. Limkumnerd and J. P. Sethna, *Phys. Rev. B* **75**, 224121 (2007).
⁴⁶ In Fourier space, the zero mode of β^P can not be obtained from the GND density field. In the context of the correlation function of β^P , the zero mode is eliminated because we subtract fields at different sites before correlating.
⁴⁷ J. M. Rickman and J. Viñals, *Philos. Mag. A* **75**, 1251 (1997).
⁴⁸ A. Roy and A. Acharya, *J. Mech. Phys. Solids* **54**, 1711 (2006).
⁴⁹ S. Varadhan, A. Beaudoin, and C. Fressengeas, in *Proceedings of Science, SMPRI2005* (2006), p. 004.
⁵⁰ D. Kuhlmann-Wilsdorf and N. Hansen, *Scr. Metall. Mater.* **25**, 1557 (1991).
⁵¹ D. A. Hughes and N. Hansen, *Metall. Trans. A* **24**, 2022 (1993).
⁵² J. P. Hirth and J. Lothe, *Theory of Dislocations* (Wiley, New York, 1982).
⁵³ I. Mura, *Int. J. Eng. Sci.* **1**, 371 (1963).
⁵⁴ Stefano Zapperi and Michael Zaiser (private communication).
⁵⁵ S. Limkumnerd and J. P. Sethna, *J. Mech. Phys. Solids* **56**, 1450 (2008).
⁵⁶ A. Kurganov, S. Noelle, and G. Petrova, *SIAM J. Sci. Comput.* **23**, 707 (2001).
⁵⁷ A. Pumir and E. D. Siggia, *Phys. Fluids A* **4**, 1472 (1992).
⁵⁸ A. Pumir and E. D. Siggia, *Phys. Rev. Lett.* **68**, 1511

- (1992).
- ⁵⁹ W. Choi, Y. S. Chen, S. Papanikolaou, and J. P. Sethna, (manuscript in preparation).
- ⁶⁰ C. Song, S. Havlin, and H. A. Makse, *Nature* **433**, 392 (2005).
- ⁶¹ M. Vergassola, B. Dubrulle, U. Frisch, and A. Noullez, *Astron. Astrophys.* **289**, 325 (1994).
- ⁶² P. J. E. Peebles, *Principles of Physical Cosmology* (Princeton University Press, Princeton, 1993).
- ⁶³ P. Coles and F. Lucchin, *Cosmology: the Origin and Evolution of Cosmic Structures* (Wiley, Chichester, 1995).
- ⁶⁴ In these analyses of TEM micrographs, the authors must use an artificial cut-off to facilitate the analysis. This arbitrary scale obscures the scale-free nature behind the emergent dislocation patterns.
- ⁶⁵ D. Kuhlmann-Wilsdorf, *Mater. Sci. Eng.* **86**, 53 (1987).
- ⁶⁶ M. C. Miguel, A. Vespignani, S. Zapperi, J. Weiss, and J. R. Grasso, *Nature* **410**, 71 (2001).
- ⁶⁷ D. M. Dimiduk, C. Woodward, R. LeSar, and M. D. Uchic, *Science* **312**, 1188 (2006).
- ⁶⁸ M. D. Uchic, D. M. Dimiduk, J. N. Florando, and W. D. Nix, *Science* **305**, 986 (2004).
- ⁶⁹ J. H. Schmitt, J. V. Fernandes, J. J. Gracio, and M. F. Vieira, *Mater. Sci. Eng. A* **147**, 143 (1991).
- ⁷⁰ A. B. Lopes, F. Barlat, J. J. Gracio, J. F. Ferreira Duarte, and E. F. Rauch, *Int. J. Plasticity* **19**, 1 (2003).
- ⁷¹ T. Mura, *Micromechanics of Defects in Solids* (Kluwer Academic Publishers, Dordrecht, 1991), 2nd ed.